RNA-binding protein Rnc1 regulates cell length at division and acute stress response in fission yeast through negative feedback modulation of the stress activated MAP kinase pathway.

Running tittle:

RBP Rnc1 down-regulates stress activated MAPK activity

Francisco Prieto-Ruiz [a], Jero Vicente-Soler [a], Alejandro Franco [a], Elisa Gómez-Gil [a], Marta Sánchez-Marinas [b], Beatriz Vázquez-Marín [a], Rosa Aligué [b], Marisa Madrid [a], Sergio Moreno [c], Teresa Soto [a] # and José Cansado [a] #.

[a] Yeast Physiology Group, Departmento de Genética y Microbiología, Facultad de Biología. Universidad de Murcia. 30071 Murcia, Spain.

[b] Department of Biomedical Sciences, Facultat de Medicina. Universidad de Barcelona. 08036 Barcelona, Spain.

[c] Instituto de Biología Funcional y Genómica (IBFG), Consejo Superior de Investigaciones Científicas, Universidad de Salamanca, 37007 Salamanca, Spain.

To whom correspondence should be addressed:

José Cansado, Department of Genetics and Microbiology, Universidad de Murcia, 30071 Murcia, Spain. Tel: +34868884953; Email: jcansado@um.es

Teresa Soto, Department of Genetics and Microbiology, Universidad de Murcia, 30071 Murcia, Spain. Tel: +34868884393; Email: teresaso@um.es

Abstract word count: 200

Text word count: aprox. 7000

ABSTRACT

RNA-binding proteins (RBPs) play a major role during control of mRNA localization, stability, and translation, and are central to most cellular processes. In the fission yeast *Schizosaccharomyces pombe* the multiple K homology (KH) domain RBP Rnc1 downregulates the activity of the cell integrity pathway (CIP) via stabilization of *pmp1+* mRNA, which encodes the Pmp1 phosphatase that inactivates Pmk1, the MAPK component of this signaling cascade. However, Rnc1 likely regulates the half-life/stability of additional mRNAs. We show that Rnc1 down-regulates the activity of Sty1, the MAPK of the stress-activated MAPK pathway (SAPK), during control of cell length at division and recovery in response to acute stress. Importantly, this control strictly depends on Rnc1 ability to bind mRNAs encoding activators (Wak1 MAPKKK, Wis1 MAPKK) and downregulators (Atf1 transcription factor, Pyp1 and Pyp2 phosphatases) of Sty1 phosphorylation through its KH domains. Moreover, Sty1 is responsible for Rnc1 phosphorylation *in vivo* at multiple phospho-sites during growth and stress, and these modifications trigger Rnc1 for proper binding and destabilization of the above mRNA targets. Phosphorylation by Sty1 prompts Rnc1-dependent mRNA destabilization to negatively control SAPK signalling, thus revealing an additional feedback mechanism that allows precise tuning of MAPK activity during unperturbed cell growth and stress.

IMPORTANCE

Control of messenger RNA (mRNA) localization, stability, turnover, and translation by RNA binding proteins (RBPs) influences essential processes in all eukaryotes, including signaling by mitogen-activated protein kinase (MAPK) pathways. We describe that in the fission yeast *Schizosaccharomyces pombe* the RBP Rnc1 negatively regulates cell length at division during unperturbed growth and recovery after acute stress by reducing the activity of the MAPK Sty1 that regulates cell growth and differentiation during environmental cues. This mechanism relies on Rnc1 binding to specific mRNAs encoding both enhancers and negative regulators of Sty1 activity. Remarkably, multiple phosphorylation of Rnc1 by Sty1 favours RBP binding and destabilization of the above mRNAs. Thus, post-transcriptional modulation of MAP kinase signaling by RNA-binding proteins emerges as a major regulatory mechanism that dictates the growth cycle and cellular adaptation in response to the changing environment in eukaryotic organisms.

INTRODUCTION

RNA-binding proteins (RBPs) assemble into different mRNA-protein complexes and play key roles in post-transcriptional processes in eukaryotes, including splicing regulation, mRNA transport and modulation of mRNA translation and decay (1). The K-homology domain (KH) is found as multiple copies in many eukaryotic RBPs that coordinate the different steps of RNA synthesis, metabolism and localization (2). Eukaryotic type I KH domains share a minimal βααβ structure with two additional α and β strands folded in a C-terminal orientation to this core motif (3). A conserved GXXG loop located between α1 and α2 helices is essential for RNA recognition and docking by KH domain-containing RBPs, and mutations in this motif fully impair its nucleic acid binding ability (2, 3).

Like all eukaryotes, the fission yeast *Schizosaccharomyces pombe* possess a large number of putative RBPs (~140), many of which (~60%) are encoded by non-essential genes (4). Among them, Rnc1 is a KH-domain non-essential RBPs that have been functionally characterized in this organism (5, 6). A main *in vivo* target for Rnc1 is *pmp1*+ mRNA, which encodes the dual specificity phosphatase Pmp1 that specifically dephosphorylates and inactivates MAPK Pmk1, the core member of the cell integrity pathway (CIP) in fission yeast (5, 7). Rnc1 negatively regulates CIP signaling via stabilization of *pmp1*+ mRNA; consequently, combined mutation of the GXXG loops within each of its three KH domains results in abrogated mRNA binding and a lack of function phenotype similar to Rnc1 deletion (8). Moreover, activated Pmk1 binds and phosphorylates Rnc1 *in vivo* at a MAPK consensus phospho-site located at a threonine residue at position 50, and this post-translational modification enhances the activity of Rnc1 to bind and stabilize Pmp1 mRNA, thus posing Rnc1 as a negative feedback loop of MAPK signaling (5, 6). However, besides *pmp1*+ mRNA, to date no other mRNAs have been shown to be regulated by Rnc1 *in vivo*.

Intriguingly, a systematic comparative transcriptomic analysis has revealed that, with respect to wild type cells, the number of up-regulated genes in vegetatively growing *rnc1*Δ cells is much larger than those that become down-regulated (77 versus 27) (4), suggesting that Rnc1 may also negatively regulate the mRNA half-life/stability of specific transcripts.

The stress-activated MAPK pathway (SAPK) plays an essential role during the control of cell cycle and the general response to stress in *S. pombe* (Fig. 1A) (7). Once activated by dual phosphorylation at two conserved threonine and tyrosine residues by the MAPKK Wis1, Sty1, the core MAPK component of the module, moves to the nucleus and phosphorylates the bZIP domain transcription factor Atf1 to modulate the expression of the CESR (Core Environmental Stress Response) genes, which participate in the consequent adaptive cell response (Fig. 1A) (9). Besides Atf1, activated Sty1 phosphorylates multiple nuclear and/or cytoplasmic substrates, including Srk1 kinase and polo kinase Plo1, to regulate cell cycle progression at the G2/M transition during growth and stress (7, 10). Activated Sty1 also phosphorylates Csx1, a RBP that associates with and stabilizes *atf1*$^{+}$ mRNA to modulate the expression of Sty1- and Atf1-dependent genes during oxidative stress, and is critical for cell survival under this specific condition (11). Importantly, both the SAPK and CIP pathways functionally crosstalk, since the Sty1-tyrosine phosphatases Pyp1 and Pyp2 and serine/threonine phosphatases Ptc1 and Ptc3, whose transcriptional induction is dependent on the Sty1-Atf1 branch, also associate with and dephosphorylate activated Pmk1 *in vivo* (12). Thus, the SAPK pathway negatively impacts the activity of the CIP pathway through the transcriptional induction of shared MAPK-phosphatases (Fig. 1A) (12).

In this work we provide evidence to show that Rnc1 is phosphorylated by Sty1 in multiple

sites during growth and stress to elicit Rnc1 binding and destabilization of mRNA transcripts encoding several components of the SAPK pathway. This results in a reduction of Sty1 activity that ensures a precise control of cell size progression during vegetative growth and response to acute stress.

RESULTS

Reduced cell length at division of *rnc1*Δ cells results from enhanced SAPK activity. We noted that cell length at division of cells of exponentially growing mutant lacking the KH-domain RBP Rnc1 (*rnc1*Δ) is significantly reduced as compared to wild type cells (14.04 ± 0.25 *vs* 11.98 ± 0.29 µm; Fig. 1B). We constructed a *rnc1*Δ mutant in a *cdc25-22* background and synchronized the cells in G2 by arresting the *cdc25-22* mutant at 36°C during 4 h (13). In this condition, *rnc1*Δ cells displayed a clear defect in polarized growth as evidenced by a reduction in cell length as compared to control cells (Fig. 1C). Rnc1 activity is negatively regulated by the cell integrity pathway and its main effector the MAPK Pmk1 (5). However, cell length at division of either *pmk1*Δ cells or in a mutant strain lacking the dual specificity phosphatase Pmp1 that dephosphorylates and inactivates Pmk1 in *vivo* (14), and whose mRNA is positively stabilized by Rnc1 (5), was similar to that of wild type cells (Fig. 1B). Also, length at division of the double *rnc1*Δ *pmk1*Δ mutant was virtually identical to that of *rnc1*Δ cells (Fig. 1B). In fission yeast the SAPK pathway and its effector MAPK Sty1 positively regulate cell cycle at the G2/M transition (Fig. 1A) (7, 15, 16). While *sty1*Δ cells show an elongated cell morphology with increased length at division, those expressing the constitutively active MAPKK allele Wis1DD that hyperactives Sty1 show a reduced cell size at division (Fig. 1B) (7). Remarkably, Sty1 deletion completely suppressed the reduced cell length at division of *rnc1*Δ cells, while the short cell length of *rnc1*Δ *wis1DD* cells was identical to that of the *wis1DD* mutant (Fig. 1B). In addition, basal Sty1 activity

was significantly higher in exponentially growing *rnc1*Δ cells expressing a genomic C-terminal HA-tagged version of the MAP kinase, as compared to wild type cells or a *pmk1*Δ mutant (Fig. 1D). These observations strongly suggest that the reduced cell length at division of *rnc1*Δ cells during unperturbed growth is due to enhanced basal phosphorylation of MAP kinase Sty1.

mRNA and protein levels of positive and negative regulatory members of the SAPK pathway are increased in *rnc1*Δ cells. Considering the above results, we hypothesized that Rnc1 might somehow modulate Sty1 activity by regulating mRNA levels of specific SAPK components (Fig. 1A). We employed qPCR analysis to systematically and comparatively analyze mRNA expression levels of several core members of this signalling cascade in exponentially growing *rnc1*Δ cells as compared to wild type cells. Strikingly, mRNA levels of the response regulator Mcs4, the redundant MAPKKK Wak1, the MAPKK Wis1, the MAPK Sty1, the transcription factor Atf1, and the Sty1 phosphatases Pyp1, Pyp2 and Ptc1 (7) (Fig. 1A) were significantly increased in *rnc1*Δ cells as compared to wild type cells (Fig. 2A).

Quantitative Western blot analysis of strains expressing genomic epitope-tagged fusions revealed that total protein levels of Wak1, Wis1, Atf1, Pyp1 and Pyp2, but not those of Mcs4, Sty1, and Ptc1, became also upregulated in *rnc1*Δ cells with regard to wild type or *pmk1*Δ cells (Fig. 2B). Modification of the 3´UTRs of the native genes introduced for expression of the corresponding proteins as genomic C-terminal epitope-tagged fusions could have reduced or inhibited Rnc1-mRNA binding in these specific genetic backgrounds. Thus, Rnc1 down-regulates both mRNA and the ensuing protein levels of positive (Wak1, Wis1) and negative (Pyp1, Pyp2, and Ptc1) regulators of Sty1 phosphorylation. However,

*rnc1*Δ cells show a net increase in MAPK basal phosphorylation (Fig. 1D), suggesting that Rnc1-mediated downregulation of Sty1 activators might be more biologically relevant *in vivo*. Indeed, simultaneous deletion of Pyp1 tyrosine phosphatase, which dephosphorylates Sty1 *in vivo* and whose mRNA and protein levels are enhanced in *rnc1*Δ cells (Fig. 2A and B), further increased basal Sty1 phosphorylation levels in vegetatively growing *rnc1*Δ cells (*pyp1*Δ *rnc1*Δ double mutant) as compared to the single mutant counterparts (Fig. 2C). The additive rise in Sty1 activity of *rnc1*Δ *pyp1*Δ cells was accompanied by enhanced expression of Atf1 transcription factor and Pyp2 tyrosine phosphatase protein levels as compared to the single mutants (Fig. 2C). Therefore, Rnc1 prompts a decrease in mRNA levels of specific positive and negative regulators within the SAPK pathway during vegetative growth that results in a reduced Sty1 activity *in vivo*.

The SAPK pathway becomes activated and plays a main role in *S. pombe* during cell survival under multiple environmental cues including salt stress (7). We performed a comparative qPCR analysis of mRNA expression of SAPK gene members in wild type and *rnc1*Δ cells after 15 and 60 min following an osmotic saline stress with 0.6 M KCl. As shown in Fig. 3A, and confirming previous observations (9), mRNA expression levels of *mcs4*+, *wak1*+, and *wis1*+ genes decreased during saline stress in wild type cells at early incubation times (15 min), and recover thereafter. However, the drop in expression of the above genes was significantly less severe in salt-stressed *rnc1*Δ cells (Fig. 3A). Also, as compared to wild type cells, Rnc1 absence elicited a further increase in mRNA expression levels in genes encoding Atf1 transcription factor (*atf1*+), and phosphatases Pyp1, Pyp2 and Ptc1 (*pyp1*+, *pyp2*+, *ptc1*+), which reach its maximum after 15 min of treatment (*pyp2*+), or at longer incubation times (*atf1*+, *pyp1*+, *ptc1*+). Therefore, Rnc1 downregulates mRNA levels of positive and negative regulators of the SAPK pathway in

response to stress.

The overall magnitude and dynamics of Sty1 activation during saline stress increased in the *rnc1*Δ mutant as compared to wild type cells (Fig. 3B). Although expression of *wak1+* (MAPKKK) and *wis1+* (MAPKK) genes becomes downregulated in wild type cells shortly after salt stress (Fig. 3A), the respective Wak1 and Wis1 protein levels raised during this treatment, and Wis1 underwent a clear mobility shift whose origin remains unknown, as previously shown (Fig. 3C and D) (17). Again, KCl-treated *rnc1*Δ cells showed a relative increment in both Wak1 and Wis1 protein levels and mobility shift as compared to wild type cells (Fig. 3C and D). Sty1 hyperphosphorylation in salt-stressed *rnc1*Δ cells resulted in a concomitant increase in the expression levels of its downstream targets Atf1 transcription factor and the tyrosine phosphatases Pyp1 and Pyp2 (Fig. 3D). Both phosphatases, whose transcriptional induction takes place via Sty1-Atf1, are also known to dephosphorylate activated Pmk1 *in vivo* (12). We did not observe significant differences in basal Pmk1 activity between vegetatively growing wild type cells and *rnc1*Δ cells (Fig. S1). Importantly, Pmk1 activation in response to a salt stress was significantly lower in *rnc1*Δ cells with respect to wild type cells (Fig. 3F), suggesting that in this mutant enhanced expression of Pyp1 and Pyp2 reinforces the inhibitory cross-talk between the SAPK and the CIP signaling cascades. Hence, Rnc1-dependent down-regulation of mRNA levels encoding SAPK members warrants proper activation of Sty1 and Pmk1 MAPKs in response to stress.

MAPK-dependent phosphorylation of Rnc1 *in vivo* during growth and stress is strongly dependent on Sty1 function. The cell integrity pathway MAPK Pmk1 associates to and phosphorylates Rnc1 *in vivo* at a threonine residue at position 50 located within a perfect MAPK consensus phospho-site (Fig. 4A) (5). The results obtained so far suggested

that this residue might also be targeted by Sty1 *in vivo*. Co-immunoprecipitation of genomic Rnc1-3HA and Sty1-GFP fusions from yeast extracts confirmed that both proteins associate *in vivo* (Fig. 4B). We used *in vitro* thiophosphate assay to test whether an analog-sensitive Sty1 kinase allele *sty1(T97A*) directly phosphorylates Rnc1. As shown in Fig. 4B, bacterially purified GST-Sty1(T97A) activated by a constitutively active version of Wis1 MAPKK (GST-Wis1DD), was able to effectively thiophosphorylate a GST-Rnc1 fusion *in vitro*. This modification was dependent upon Sty1 kinase activity since it was totally inhibited in the presence of the specific analog-sensitive inhibitor 3BrPP1 (Fig. 4C). Importantly, as compared to wild type GST-Rnc1, thiophosphorylation of a GST-Rnc1(T50A) mutated version by Sty1 was somewhat reduced but not totally abrogated (Fig. 4C). Besides T50, Rnc1 amino acid sequence has five additional putative MAPK phosphorylation sites (T45, T171, T177, S278, and S286) (Fig. 4A). Remarkably, Sty1 failed to thiophosphorylate a Rnc1 fusion where all the six S/T residues were changed by alanine (GST-Rnc1(S/T6A)) (Fig. 4C). These results suggest that while T50 is a main phosphorylation site for Sty1 within Rnc1, other phospho-sites are likely targeted by this kinase *in vivo*.

We found that a genomic Rnc1-3HA fusion migrates during unperturbed vegetative growth in SDS-PAGE as a doublet that undergoes a partial mobility shift during a nutritional stress in absence of glucose (Fig. 4D). Phosphatase lambda treatment of glucose-limited cell extracts in the presence/absence of a phosphatase specific inhibitor revealed that Rnc1 mobility shift is due to phosphorylation (Fig. 4E). Remarkably, phosphorylated species were not detected in cells expressing a Rnc1(S/T6A)-3HA fusion in the absence of the sugar (Fig. 4D). Hence, these shifted bands represent a subset of Rnc1 MAPK-phosphorylated species, and can be employed as readout to follow Rnc1 phosphorylation by MAPKs under different biological contexts. Despite their low abundance during asynchronous unperturbed

growth, Rnc1 MAPK-phophorylated species were enriched during the M phase of cell cycle as evidenced in cells arrested in a *nda3-km311* background (Fig. 4F). MAPK phosphorylation of Rnc1 was minimal during G2-arrest in a *cdc25-22* background, increased progressively after release during mitosis and G1/S phases, and decreased again as cell entered into G2 (Fig. 4G). Remarkably, this phosphorylation pattern was also conserved in G2-released *cdc25-22 pmk1*Δ cells (Fig. 4G). Although we could not follow Rnc1 phosphorylation in a *sty1*Δ background because Sty1 deletion negatively interferes with G2 arrest in the *cdc25-22* background (15), the above results suggest that Sty1 is mostly responsible for the cell cycle-dependent phosphorylation of Rnc1.

Similar to glucose deprivation, both Sty1 and Pmk1 become activated in *S. pombe* in response to other stimuli including heat stress or in the presence of arsenite (18, 19). As can be seen in Fig. 4H, MAPK-dependent phosphorylation of Rnc1 was detected with different magnitudes and dynamics in wild type cells in response to each of the above stressors. Importantly, Sty1 absence elicited a major reduction in Rnc1 phosphorylation under all the conditions analyzed (Fig. 4H). On the contrary, the impact of Pmk1 deletion on Rnc1 phosphorylation was somewhat evident in the absence of glucose but it was virtually inexistent under the remaining stimuli (Fig. 4H). Taken together, these results indicate that Sty1 is the main MAPK that phosphorylates Rnc1 *in vivo*, both during unperturbed growth and in response to stress.

Rnc1 binds to mRNAs encoding SAPK components to promote their destabilization *in vivo*. RBP´s recognise and bind target mRNA molecules in sequence dependent as well as independent manner, and promote either their degradation or stabilization (20). In has been shown that a double mutation in the hallmark GxxG loop (GxxG to CDDG) impairs

nucleic acid binding of KH domains without compromising their stability (2). Therefore, we constructed a mutant Rnc1 version where the two residues within each of the three conserved GXXG loops of the respective KH domains are replaced by aspartic acid (Rnc1(m3KH)). We expressed in *S. pombe* N-terminal GST-fused versions of wild type and mRNA binding defective Rnc1 (m3KH). GST alone and the purified fusions were then mixed with fission yeast total RNA, and, after incubation with Glutathione-Sepharose beads and extensive washing, the bound mRNA´s were subjected to RT-qPCR analysis to quantify those encoding SAPK components. As shown in Fig. 5A, *wak1+, wis1+, atf1+, pyp1+,* and *pyp2+* mRNAs co-purified and were selectively enriched to different ratios (10X to 60X) with wild type GST-Rnc1 as compared to the GST-Rnc1(m3KH) mutated version, suggesting that KH domains mediate Rnc1 binding to mRNAs of SAPK components *in vitro*. As compared to control Rnc1-3HA cells, *wak1+*, *wis1+* and *pyp1+* mRNAs levels, but not those of *atf1+* and *pyp2+*, increased significantly in growing cells expressing a genomic Rnc1 fusion lacking mRNA binding ability (Rnc1(m3KH)-3HA) (Fig. 5B). Wak1, Wis1 and Pyp1 protein levels were also higher in Rnc1(m3KH)-3HA cells, whereas Atf1 levels remained unchanged (Fig. 5C). Although *pyp2+* mRNA levels were almost identical in control and m3KH cells, Pyp2 protein levels increased ~2 times in the mutant background (Fig. 5C), but it was of a lower magnitude than that in *rnc1*Δ versus wild type cells (~8-9 times) (Fig. 2C). It may be possible that Rnc1-m3KH is still able to bind *atf1+* and *pyp2+* mRNAs to some extent. Alternatively, the Rnc1-3HA fusion used in these constructs might be not fully functional. In support for this hypothesis, both basal Sty1 phosphorylation and cell length at division were slightly increased and reduced, respectively, in Rnc1-3HA cells with respect to the parental strain expressing wild type (unfused) Rnc1 (Fig. S2). In any case, and like *rnc1*Δ cells, Rnc1(m3KH)-3HA cells also displayed enhanced basal Sty1 activity (Fig. 5D) and decreased cell length at division (Fig. 5E) with respect to the isogenic

wild type counterpart.

As compared to control cells, Sty1 activation and Atf1 protein levels did not rise significantly in response to a saline osmotic stress in Rnc1-m3KH cells lacking mRNA binding ability (Fig. 6A). In contrast, they showed a reproducible increase in protein expression of MAPKKK Wak1, MAPKK Wis1 and tyrosine phosphatases Pyp1 and Pyp2 relative to control cells (Fig. 6A), and a marked reduction in Pmk1 activation when subjected to an identical treatment (Fig. 6A). Altogether, these findings suggest that downregulation of Sty1 activity by Rnc1 relies on its ability to bind specific mRNAs (*wak1+, wis1+*, *pyp1+*, *pyp2+*) encoding components of the SAPK pathway. However, if this hypothesis is correct, Rnc1 binding should decrease the stability of these mRNAs. To explore this possibility, exponentially growing cultures of Rnc1-3HA (wild type) and Rnc1(m3KH)-3HA cells were treated with 250 µg/ml of 1,10 phenantroline to block transcription (11); total RNAs were extracted at different times, and the decay in mRNA levels of SAPK transcripts was determined by RT-qPCR analysis (see Materials and Methods). As shown in Fig. 5D, the half-lives of either *wak1+, pyp1+, wis1+,* and *pyp2+* mRNAs were significantly higher in Rnc1(m3KH)-3HA cells as compared to wild type cells, suggesting that Rnc1 binding promotes their destabilization *in vivo*.

MAPK-dependent phosphorylation of Rnc1 *in vivo* is essential to negatively regulate Sty1 activity during control of cell length at division and adaptive response to acute stress. The observation that Sty1 phosphorylates Rnc1 *in vivo* at multiple S/T residues during unperturbed growth and stress (Fig. 4), prompted us to further evaluate the impact of this post-translational modification on its function as a RBP. A non-phosphorylatable GST-Rnc1 fusion (GST-Rnc1(S/T6A)) expressed in fission yeast was several times less effective

that the wild type (GST-Rnc1) in binding *wak1*+, *wis1*+, *atf1*+, *pyp1*+, and *pyp2*+ mRNAs *in vitro* (Fig. 5A). Moreover, *S. pombe* cells expressing a genomic non-phosphorylatable HA-fused Rnc1 mutant version (Rnc1(S/T6A)-3HA), were phenotypically similar to those defective in mRNA-binding (Rnc1(m3KH)-3HA), as they showed increased mRNA levels (Fig. 5B) and half-lives (Fig. 6B) of *wak1+, wis1*+ and *pyp1+,* and enhanced expression of Wak1, Wis1 and Pyp1 proteins during unperturbed growth (Fig. 5C) and in response to stress (Fig. 6A). These phenotypes were also accompanied by a net increase in basal Sty1 activity (Fig. 5D), and reduced cell length at division (Fig. 5E). Therefore, Sty1-dependent phosphorylation impairs Rnc1 binding and destabilization of mRNAs encoding SAPK members, and the ensuing reduction in MAPK activity to control cell length at division during growth and stress.

In *S. pombe* the SAPK pathway and its core member Sty1 MAPK controls multiple cellular events including cell survival in response to environmental cues (7). Many of these adaptive responses are executed through a transcriptional program involving expression of Atf1-dependent genes (9). Consequently, ***sty1*Δ** cells show strong growth sensitivity when facing different stressors, including high temperature, saline stress (KCl, NaCl), oxidative stress (hydrogen peroxide), or caffeine (7, 21, 22) (Fig. S3).The observation that mutants lacking Rnc1 display enhanced Sty1 activity and Atf1 expression, suggested that this situation might favour cellular adaptation and survival in response to environmental stress. However, growth sensitivity of *rnc1*Δ cells was virtually identical to that of wild type cells in response to the above treatments (Fig. S3), suggesting that Rnc1 does not play a significant role in the adaptive cellular response to stress. Remarkably, we found that, as compared to control cells, *rnc1Δ* cells exhibited a significant increase in growth recovery after being subjected to an acute thermal stress (55ºC) during 60-90 min, and this phenotype was shared by both

Rnc1(m3KH)-3HA and Rnc1(S/T6A)-3HA cells (Fig. 6C). Moreover, Sty1 absence completely suppressed the enhanced growth recovery phenotype of *rnc1Δ* cells (Fig. 6C). Taken together, these results suggest that Sty1-dependent phosphorylation triggers Rnc1-mRNA binding to negatively regulate *S. pombe* cell growth and survival in response to acute stress (Fig. 6D).

DISCUSSION

In this work we show that the KH-domain RBP Rnc1 down-regulates SAPK function it *S. pombe* during control of cell length at division and the adaptive response to acute stress (Fig, 6D). This assumption is based in the finding that, as compared to wild type cells, *rnc1Δ* cells display increased basal Sty1 activity that results in a reduction in length at division and enhanced growth recovery after acute thermal stress. Importantly, Rnc1 negative control of SAPK function is strictly dependent on its ability to bind mRNAs encoding both activators (Wak1 MAPKKK, Wis1 MAPKK) and negative regulators (Atf1 transcription factor, Pyp1 and Pyp2 tyrosine phosphatases) of Sty1 phosphorylation through its KH domains. Consequently, cells expressing a KH-domain mutated version of the RBP unable to bind mRNA (Rnc1-m3KH) phenocopied *rnc1Δ* cells and showed increased Sty1 activity, reduced cell length at division, and enhanced tolerance to heat shock. As a whole, our observations depict a new role for Rnc1 as a negative modulator of SAPK function in fission yeast (Fig. 6D).

This novel mechanism seems unrelated to Rnc1 downregulation of CIP signaling, which relies in its ability to bind and stabilize *pmp1+* mRNA encoding the dual-specificity phosphatase Pmp1 that dephosphorylates and inactivates Pmk1 *in vivo* (5). Indeed, our results suggest that Rnc1 binding prompts instead the destabilization of specific mRNAs

encoding core upstream and downstream components of the SAPK cascade including at least *wak1*+, *wis1*+ and *pyp1*+. This assumption is sustained by the increased expression and half-lives of these mRNAs found in Rnc1-m3KH cells during unperturbed growth relative to wild type cells. Signal transmission to Wis1 during growth and saline stress is mediated by a Wak1–Win1 MAPKKK heteromer complex stabilized by Mcs4 (17). We thus propose that in *rnc1*Δ cells the enhanced expression of *wak1*+ and *wis1*+ mRNAs, which results in increased availability Wak1 and Wis1 proteins, allows for a more efficient downstream transmission from this module and the ensuing activation of Sty1 MAPK. Indeed, the RBP-mediated negative control *wak1*+ and *wis1*+ mRNAs seems more biologically relevant than downregulation of *atf1*+, *pyp1*+ and *pyp2*+ mRNAs, as *rnc1*Δ cells display a net increase in MAPK activity. Moreover, although enhanced expression of *mcs4*+, *sty1*+ and *ptc1*+ mRNAs in *rnc1*Δ cells was not accompanied by a parallel increase in the respective protein levels expressed as C-terminal tagged fusions, the possibility that Rnc1-dependent downregulation of Mcs4, Sty1 and Ptc1 expression also impinges SAPK signalling cannot be ruled out. Previous global RNAseq analysis showed that the number of up-regulated genes in vegetatively growing *rnc1*Δ cells (including *pyp1*+, which has been confirmed in this work to be a direct target for Rnc1), is larger than those being down-regulated (4). Thus, it seems highly likely that the role of Rnc1 as negative regulator of mRNAs half-life/stability is extended to other mRNAs than those encoding SAPK components.

Increased mRNA expression of *wak1*+, *wis1*+ and *pyp1*+ genes in *rnc1*Δ and Rnc1-m3KH cells resulted in the ensuing rise in Wak1, Wis1 and Pyp1 protein levels not only during vegetative growth, but also in response to stress, suggesting that Rnc1 binding to the those mRNAs regulates SAPK function in response to a variety of environmental cues. In

response to Sty1 activation, Atf1 transcription factor elicits expression of many CESR genes including *pyp1*+ and *pyp2*+ (9). In this context, it could be possible that the enhanced levels of Atf1 present in *rnc1*Δ cells could account for the increased expression of the remaining SAPK members described in this work. However, this possibility seems highly unlikely for two main reasons. First, mRNA and protein expression levels of *wak1*+, *wis1*+, *pyp1*+ and *pyp2*+ significantly increased in cells expressing a Rnc1 mutant version unable to bind mRNAs (Rnc1(m3KH)-3HA) with respect to wild type cells. Importantly, Atf1 levels did not change in this background (Fig. 5B and 5C). Second, *wak1*+, *wis1*+, *pyp1*+ and *pyp2*+ mRNAs co-purified and became selectively enriched with wild type Rnc1 (Fig. 5A), and their half-lives increased in absence of Rnc1 function (Fig. 6B). Therefore, Rnc1-mediated downregulation of mRNAs encoding the above SAPK components involves direct binding and destabilization by the RBP, and is independent of the altered expression pattern of Atf1.

While Pmk1 is a specific substrate for Pmp1 phosphatase, Pyp1 and Pyp2 dephosphorylate both Sty1 and Pmk1 *in vivo* during growth and stress (12). The finding that the magnitude of Pmk1 activation during an osmotic saline stress is strongly reduced in the *rnc1*Δ mutant as compared to wild type cells, further confirms the role of Rnc1 as a negative regulator of SAPK signalling and Pyp1/2 expression. It also shows its relevance as an additional player whereby SAPK may decrease CIP signalling in response to environmental stimuli.

Post-translational modification by phosphorylation has a major influence on RBP function and affinity toward their targets, with the consequent positive or negative impact on mRNA stability, turnover and translation efficiency (23, 24). *In vivo* Rnc1 phosphorylation by Pmk1 at a putative MAPK phospho-site located at T50 enhances RBP binding and stabilization of

Pmp1 mRNA (5). However, in this work we show that Sty1 associates *in vivo* and phosphorylates Rnc1 not only at T50 but at additional MAPK phospho-sites (T45, T171, T177, S278, and/or S286), whose precise identity remains to be determined. During unperturbed growth, a very small fraction of the total Rnc1 protein becomes phosphorylated at these sites in wild type cells particularly during the M and G1/S phases of the cell cycle. However, Rnc1 phosphorylation is much more evident when cells are subjected to treatments that activate either Sty1, like arsenite (25), or both Sty1 and Pmk1, like glucose deprivation or thermal stress (7, 18, 26). Remarkably, enhanced MAPK-dependent phosphoryation of Rnc1 was mostly absent in *sty1Δ* cells but not in *pmk1Δ* cells during vegetative growth and in response to the above stresses. These results strongly suggest that Sty1 is a main responsible for Rnc1 phosphorylation during growth and in response to environmental cues. Moreover, the finding that the phenotypes of Rnc1-S/T6A cells lacking phosphorylatable MAPK sites (reduced cell length at division, enhanced Sty1 activity and activation under stress, and increased cell recovery after acute thermal shock), mimic those of cells expressing the mutant version unable to bind mRNA (Rnc1-m3KH), strongly suggests that Sty1-dependent phosphorylation triggers Rnc1 for proper binding and destabilization of several of its mRNA substrates (*wis1*+, *pyp1*+,..).

How can phosphorylated Rnc1 promote either mRNA stabilization or destabilization? An attractive possibility is that alternative phosphorylation of Rnc1 by Sty1 and/or Pmk1 at one or several S/TP sites might trigger its function as an mRNA stabilizer or destabilizer depending on the environmental context. Protein-RNA interactions were initially thought to be mostly mediated by canonical RNA-binding regions, like KH domains, that form stable secondary and tertiary structures. However, recent studies, including proteome-wide data, have revealed unexpected roles for intrinsically disordered protein regions in RNA binding

(27). Interestingly, all of the Rnc1 MAPK phosphorylation sites (T50, T45, T171, T177, S278, and S286) are excluded from KH domains and lie within predicted intrinsically disordered regions of the protein (Fig. 4B). Alternative phosphorylation at these sites might thus elicit major changes in Rnc1 conformation and affect its ability to bind mRNAs with different affinity. The stabilizer/destabilizer role for Rnc1 might also be imposed by specific structural features of its target mRNAs. Rnc1 binds to several UCAU repeats in the 3′-UTR of *pmp1*+ mRNA, while mutation at these sequences impedes Rnc1 binding and prompts mRNA destabilization (5, 6). These repeats belong to the consensus YCAY RNA binding element that is bound by KH-domain RBPs like the mammalian onconeural antigen Nova-1 (28). However, in contrast to the high number of UCAU motifs found in the long *pmp1*+ 3´-UTR, they have a scarce presence in the shorter *wak1*+ (0), *wis1*+ (1), *atf1*+ (2), *pyp1*+ (0), and *pyp2*+ (3) 3´-UTRs (Fig. S4). In addition, the possibility that Rnc1 binds to those mRNAs via UCAU motifs located at their ORFs or 5´UTRs, or through other unknown motifs, cannot be discarded.

From a biological perspective, the existence of a shared control of Rnc1 function by two MAP kinases (Sty1 and Pmk1), should somehow be expected when considering that both SAPK and CIP pathways crosstalk extensively in *S. pombe* and become activated by a similar range of stimuli (7). Therefore, alternative Rnc1 phosphorylation by both SAPK and CIP signalling cascades might allow for exquisite differential regulation of their biological functions during unperturbed growth and in response to changing environmental conditions.

MATERIAL AND METHODS

Strains, growth conditions and reagents. The S. *pombe* strains used in this work are listed in Table S1. They were routinely grown with shaking at 28 or 30ºC in rich (YES) or

minimal (EMM2) medium with 2% glucose, and supplemented with adenine, leucine, histidine, or uracil (100 mg/L, Sigma-Aldrich) (13). In stress experiments log-phase cultures (OD_{600}= 0.5; ~10^6 cells/ml) were either incubated at 40ºC (heat shock), or supplemented with KCl (Sigma-Aldrich) or sodium arsenite (Sigma-Aldrich). In glucose starvation experiments cells grown in YES medium with 7% glucose were recovered by filtration, and resuspended in the same medium lacking glucose and osmotically equilibrated with 3% glycerol. At different times the cells from 50 ml of culture were harvested by centrifugation at 4ºC, washed with cold PBS buffer, and the yeast pellets immediately frozen in liquid nitrogen for further analysis. Transformants expressing GST-fused Rnc1 constructs from pREP3X-based plasmids were grown in liquid EMM2 medium with thiamine (5 mg/L), and transferred to EMM2 lacking thiamine for 24h.

Gene disruption, epitope tagging, site-directed mutagenesis, and expression of GST-tagged Rnc1 fusions. *S. pombe rnc1*$^+$ null mutant was obtained by ORF deletion and replacement with the G418 (*kanR*) cassette by PCR-mediated strategy using plasmid pFA6a-*kanMX6* (29) and the oligonucleotides Rnc1D-FWD and Rnc1D-REV (Table S2). Plasmid pFA6a-3HA-*KanMX6* and the oligonucleotides Rnc1-CT-FWD and Rnc1-CT-REV were employed to obtain a genomic C-terminal Rnc1-3HA tagged version. Strains expressing different genomic fusions in multiple genetic backgrounds were constructed either by transformation or after random spore analysis of appropriate crosses in SPA medium.

To construct the template plasmid pTA-Rnc1:HA, the *rnc1*$^+$ C-terminal HA tagged ORF plus regulatory sequences, the *KanMX6* cassette, and 3' UTR were amplified by PCR using genomic DNA from Rnc1-3HA cells as template, and the 5′-oligonucleotide Rnc1-FWD, which hybridizes –421–391 bp upstream of the *rnc1*$^+$ start codon, and the 3′-oligonucleotide

Rnc1-REV, which hybridizes +788+818 bp downstream of the *rnc1*$^{+}$ stop codon. The PCR fragment was cloned into plasmid pCR2.1 using the TA cloning kit (Thermo Fisher Scientific) and confirmed by sequencing. Rnc1:HA (T50A) mutant was obtained by one-step site-directed mutagenesis PCR using plasmid pTA-Rnc1:HA as a template and the correspondent mutagenic oligonucleotide pairs Rnc1-T50A-FWD and Rnc1-T50A-REV (30). To obtain plasmids pTA-Rnc1(K110D, A111D, R196D, N197D, R338D, G339D):HA (synonymous to Rnc1(mKH):HA; Rnc1 mutated at the 3 KH mRNA binding domains) and pTA-Rnc1(T45A, T50A, T171A, T177A, S278A, S286A):HA (synonymous to Rnc1(S/T6A):HA; Rnc1 mutant lacking MAPK phospho-sites), plasmid pTA-Rnc1:HA was digested with *Sac*I and *Pac*I, and the released *rnc1*+ ORF fragment was substituded with synthesized DNA fragments including the indicated mutations (GenParts; GenScript) and digested with *Sac*I and *Pac*I. The above plasmids were used as PCR templates to obtain the corresponding DNA fragments which were transformed into wild type strain MM1. Transformants G418 resistant were obtained, and the correct integration of the respective genomic wild type (Rnc1-3HA) and mutated (Rnc1(T50A)-3HA; Rnc1(mKH)-3HA; and Rnc1(S/T6A)-3HA) fusions was verified by both PCR and Western blot analysis. Incorporation of the mutagenized residues was confirmed by sequencing.

Bacterially expressed GST-Rnc1, GST-Rnc1(T50A), GST-Rnc1(mKH), and GST-Rnc1(S/T6A) fusions were obtained by PCR employing pTA-Rnc1:HA, pTA-Rnc1(T50A):HA, pTA-Rnc1(mKH):HA, and pTA-Rnc1(S/T6A):HA plasmids as templates, respectively, and the oligonucleotides GSTRnc1-FWD-*Bam*HI and GSTRnc1-REV-*Xba*I. The PCR products were then digested with *Bam*HI and *Xba*I and cloned into plasmid pGEX-KG. To express the GST-Rnc1 fusions in *S. pombe* under the control of the strong version of the thiamine (B1) repressible promoter from pREP3X expression plasmid (31),

wild-type and mutagenized Rnc1constructs were by amplified by PCR employing plasmids and pTA-Rnc1:HA, pTA-Rnc1(T50A):HA, pTA-Rnc1(mKH):HA, and pTA-Rnc1(S/T6A):HA plasmids as templates, and the oligonucleotide pair GST-FWD-*Xho*I and GSTRnc1-REV-*Sma*I. PCR Fragments were digested with *Xho*I and *Sma*I and cloned into pREP3X. GST ORF (negative control) was also cloned into pREP3X by employing pGEX-KG plasmid as template and the oligonucleotides GST-FWD-*Xho*I and GST-REV-*Bam*HI. They were separately transformed into *S. pombe*, and *leu1*$^{+}$ transformants were selected in EMM2 medium plus thiamine.

cDNA synthesis and quantitative real time polymerase chain reaction (qPCR). *S. pombe* wild type and mutant strains were grown in YES medium to a final OD_{600}= 0.5; (~10^6 cells/ml). Total RNAs were purified using the RNeasy mini kit (Qiagen), treated with DNase (Invitrogen), and quantitated using Nanodrop 100 spectrophotometer (ThermoScientific). Total RNAs (1 µg) were reverse transcripted into cDNA with the iScript reverse transcription supermix (BioRad). Quantitative real time polymerase chain reactions (qPCR) were performed using the iTaq Universal SYBR Green Supermix and a CFX96 Real-Time PCR system (Bio-Rad Laboratories, CA, USA). Relative gene expression was quantified based on $2^{-\Delta\Delta CT}$ method and normalized using *leu1*$^{+}$ mRNA or 28S rRNA expression in each sample. The list of gene-specific primers for qPCR is indicated in Table S2.

mRNA-Rnc1 binding assay. RNA-protein binding assays were carried out by following the method described by Satoh *et al*. (2017) with slight modifications. Exponentially growing cells (4 × 10^8 total cells) expressing N-terminal glutathione *S*-transferase (GST) tagged wild type or mutated Rnc1 proteins were disrupted in 500 µl extraction buffer (30 mM Tris HCl pH 8, 1% Triton X100, 2 mM EDTA, 1 mM dithiothreitol (DTT), plus protease and

phosphatase inhibitor cocktails (obtained from Sigma–Aldrich and Roche Molecular Biochemicals, respectively). Glutathione Sepharose 4B (GE Healthcare, USA) was added to the cleared extracts, which were incubated for 2 h at 4°C. Sepharose was washed seven times in wash buffer (30 mM Tris HCl pH 8, 1% Triton X100, 2 mM EDTA, 1 mM DTT, 3 M NaCl plus phosphatase inhibitor cocktail), and two times in binding buffer (30 mM Tris HCl pH 8, 1% Triton X100 and 1 mM DTT). Fission yeast total RNA (100 µg) and 100 U ml^{-1} SUPERase RNase inhibitor (Invitrogen) were added to the washed Sepharose containing equivalent amounts of the purified GST-Rnc1fusion, and incubated for 2 h at 4°C. After two washes in binding buffer, the RNA bound to Sepharose was extracted with the RNeasy Mini Kit (QIAGEN, Germany). cDNA synthesis (10 µl RNA) and qPCR were performed as described above.

Determination of mRNA stability. Cells were grown at 28°C in EMM2 medium to mid log phase ($OD_{660\ nm}$=0.4), and then 1,10 phenanthroline dissolved in 100% ethanol (Sigma-Aldrich) was added to cultures to a final concentration of 250 µg ml^{-1} to inhibit transcription (11). The cells from 20 ml of culture (10^8 total cells) were harvested and total RNA was extracted at the indicated time points. cDNA synthesis and determination of the relative mRNA expression levels by qPCR were performed as described above.

Detection and quantification of total and activated Pmk1 and Sty1 levels. Preparation of cell extracts, affinity chromatography purification of HA-tagged Pmk1 or Sty1 with Ni^{2+}-NTA-agarose beads (Qiagen), and SDS-PAGE was performed as described (32). This approach strongly reduces the potential inaccuracy in the detection of both total and phosphorylated MAPKs. Dual phosphorylation in either Pmk1 or Sty1 was detected employing rabbit polyclonal anti-phospho-p44/42 (Cell Signaling) or rabbit monoclonal anti-

phospho-p38 (Cell Signaling), respectively. Total Pmk1 or Sty1 were detected with mouse monoclonal anti-HA antibody (12CA5, Roche Molecular Biochemicals). Immunoreactive bands were revealed with anti-rabbit or anti-mouse-HRP-conjugated secondary antibodies (Sigma-Aldrich) and the ECL system (GE-Healthcare).

Detection of Rnc1. Cells from yeast cultures were fixed and total protein extracts were prepared by precipitation with trichloroacetic acid (TCA) as previously described (33). Proteins were resolved in 10% SDS-PAGE gels and transferred to Hybond-ECL membranes. Rnc1-3HA fusions were detected employing a mouse monoclonal anti-HA antibody (12CA5, Roche Molecular Biochemicals). Rabbit monoclonal anti-PSTAIR (anti-Cdc2, Sigma-Aldrich) was used for loading control. Immunoreactive bands were revealed with anti-rabbit or anti-mouse HRP-conjugated secondary antibodies (Sigma), and the ECL system (GE-Healthcare).

Detection and quantification of Atf1 and Mcs4, Wak1, Wis1, Pyp1, Pyp2, and Ptc1-tagged fusions. Cells extracts were prepared using Buffer IP (50 mM Tris-HCl pH 7.5, 5 mM EDTA, 150 mM NaCl, 1 mM β-mercaptoethanol, 10% glycerol, 0.1 mM sodium orthovanadate, 1% Triton X-100 and protease inhibitors), and resolved in 8, 10, or 12% SDS-PAGE gels depending on the size of the fused protein. *S. pombe* Atf1 was detected with a mouse monoclonal antibody (ATF1 2A9/8) from Abcam (ab18123). Rabbit polyclonal anti-GFP (Cell Signaling) was employed to detect Mcs4-GFP. Wak1-13myc, Wis1-13myc, Pyp1-13myc, Pyp2-13myc and Ptc1-13myc fusions were detected with a mouse monoclonal anti-c-myc antibody (clone 9E10, Roche Molecular Biochemicals). Rabbit monoclonal anti-PSTAIR (anti-Cdc2, Sigma Chemical) was used for loading control.

Immunoreactive bands were revealed with anti-rabbit or anti-mouse-HRP-conjugated secondary antibodies (Sigma-Aldrich) and the ECL system (GE-Healthcare).

Co-immunoprecipitation. Whole cell extracts from the appropiate strains were prepared in lysis buffer (20 mM Tris-HCl, pH 8.0, 2 mM EDTA, 100 mM NaCl, and 0.5% NP-40, and containing a protease inhibitor cocktail (Sigma-Aldrich). Cell extracts (3mg) were incubated with Dynabeads protein G (Novex by Life Technology) bound to polyclonal anti-GFP antibody (Cell Signaling) for 2 h at 4°C. The beads were washed four times with lysis buffer, resuspended in sample buffer, and the immunoprecipitates were then analyzed by Western blot analysis with either anti-GFP or anti-HA (12CA5, Roche Molecular Biochemicals) antibodies, and followed by immunodetection with anti-mouse HRP-conjugated secondary antibody (Sigma) and the ECL system (GE-Healthcare).

Lambda phosphatase treatment. Protein dephosphorylation assays were performed essentially as previously described in (34) with slight modifications.Total protein extracts were prepared from 1.5×10^8 cells. 25 ml cultures were mixed with 2.5 ml of trichloroacetic acid 100% (w/v) and incubated on ice for 30 min. Cells were centrifuged and the pellets washed once with 10 ml of ice-cold acetone and twice with 500 µl of beating buffer (8 M urea, 50 mM ammonium bicarbonate) containing a protease inhibitor cocktail (Sigma-Aldrich). Cells were resuspended in 200 µl of beating buffer plus protease inhibitors and disrupted with 0.5 mm glass beads in a FastPrep cell disruptor for three cycles of 35 s at 5.5 m/s, 4°C. For assays, 150 µg of protein were treated with 400 U of λ-protein phosphatase (New England Biolabs) in the presence/absence of specific phosphatase inhibitor (5 mM sodium orthovanadate) for 50 min at 30°C. The reaction volume was adjusted with water to dilute the urea-containing buffer at a ratio of 1:10. Protein

607 electrophoresis was performed on 10% SDS-PAGE gels and the Rnc1-HA fusion was
608 detected as indicated.
609
610 ***In vitro* kinase assay.** GST-Wis1DD (Constitutively active MAPKK), GST-Sty1 (T97A)
611 (analog-sensitive MAPK), GST-Rnc1, GST-Rnc1(T50A) and GST-Rnc1(S/T6A) fusions
612 were purified from *E. coli* with Glutathione Sepharose 4B beads (GE Healthcare, USA).
613 After washing extensively, GST-Wis1DD, GST-Sty1 (T97A), and GST-Rnc1 substrates
614 were incubated in 20 mM Tris (pH 8), 10 mM $MgCl_2$, and 20 μM ATPγS at 30°C for 45 min
615 in the presence/absence of 20 μM of the kinase specific inhibitor BrB-PP1 (Abcam). The
616 kinase reaction was stopped by adding 20 mM EDTA, and alkylated after incubatiion at
617 room temperature with 2.5 mM p-nitrobenzyl mesylate for 1 h. Rnc1 phosphorylation was
618 detected using an antibody against thiophosphate ester (Abcam, 92570). GST fusions were
619 detected with anti-GSTantibody (GE Healthcare, USA).
620
621 **Quantification of Western blot experiments and reproducibility of results.**
622 Densitometric quantification of Western blot signals as of 16-bit .jpg digital images of blots
623 was performed using ImageJ (35). The desired bands plus background were drawn as
624 rectangles and a profile plot was obtained for each band (peaks). To minimize the
625 background noise in the bands, each peak floating above the baseline of the corresponding
626 peak was manually closed off using the straight-line tool. Finally, measurement of the
627 closed peaks was performed with the wand tool. Relative Units for Sty1 and Pmk1
628 activation were estimated by determining the signal ratio of the anti-phospho-P38 (activated
629 Sty1) and anti-phospho-P44/42 (activated Pmk1) blots with respect to the anti-HA blot (total
630 Sty1 or Pmk1) at each time point. Relative Units for total Mcs4, Wak1, Wis1, Atf1, Pyp1,
631 Pyp2, and Ptc1 levels were estimated by determining the signal ratio of the correspondent

anti-HA (total Rnc1), anti-GFP (total Mcs4), anti-Atf1, or anti-c-myc (total Wak1, Wis1, Pyp1, Pyp2 and Ptc1) blots with respect to the anti-cdc2 blot (internal control) at each time point. Unless otherwise stated, results shown correspond to experiments performed as biological triplicates. Mean relative units ± SD and/or representative results are shown. *P*-values were analyzed by unpaired Student´s *t* test.

Plate assays of stress sensitivity for growth and cell recovery after acute thermal stress. In the growth sensitivity assay *S. pombe* wild type and mutant strains were grown in YES liquid medium to OD_{600}= 0.5, and appropriate decimal dilutions were spotted per triplicate on YES solid medium or in the same medium supplemented with varying concentrations of potassium chloride, sodium chloride, hydrogen peroxide, or caffeine (all from Sigma-Aldrich). Plates were incubated at either 30 or 37ºC for 3 days and then photographed. In the growth recovery assay after acute stress, decimal dilutions of strains were spotted per triplicate on YES solid medium, the plates were allowed to dry at room temperature for 10 min, and incubated in an oven at 55ºC. The plates were removed from the oven at timely intervals (0 to 120 min), incubated for 3 days at 30ºC, and then photographed. All the assays were repeated at least three times with similar results. Representative experiments are shown in the corresponding Figures.

Microscopy analysis. Fluorescence images were obtained with a Leica DM4000B microscope equipped with a Leica DC400F camera, and processed using IM500 Image Manager software. Calcofluor white was employed for cell wall/septum as described (13). To determine cell length at division the yeast strains were grown in YES medium to an A_{600} of 0.5 and stained with calcofluor white. A minimum of 200 septated cells were scored for each strain. Three biological replicates were scored for each strain genotype.

ACKNOWLEDGEMENTS

We thank Jonathan Millar and Miguel A. Rodriguez-Gabriel for fission yeast strains, and Pilar Pérez for helpful discussions.

This work was supported by the Ministerio de Ciencia, Innovación y Universidades, Spain [Grant reference BFU2017-82423-P to J.C.]. European Regional Development Fund (ERDF) co-funding from the European Union.

J.C., T.S., R.A., and S.M. designed the studies; F.P.-R., J.V.-S., A.F., E.G.-G., M.S.-M., B.V.-M., and M.M. performed experiments; F.P.-R., J.V.-S., J.C., T.S., R.A., S.M. and M.M. analyzed the data; J.C. and T.S. wrote the paper.

We have declared that we have no conflict of interest.

REFERENCES

1. Oliveira C, Faoro H, Alves LR, Goldenberg S. 2017. RNA-binding proteins and their role in the regulation of gene expression in *Trypanosoma cruzi* and *Saccharomyces cerevisiae.* Genet Mol Biol 40:22-30.
2. Hollingworth D, Candel AM, Nicastro G, Martin SR, Briata P, Gherzi R, Ramos A. 2012. KH domains with impaired nucleic acid binding as a tool for functional analysis. Nucleic Acids Res 40:6873-6886.
3. Grishin NV. 2001. KH domain: one motif, two folds. Nucleic Acids Res 29:638-643.
4. Hasan A, Cotobal C, Duncan CD, Mata J. 2014. Systematic analysis of the role of RNA-binding proteins in the regulation of RNA stability. PLoS Genet 10:e1004684.
5. Sugiura R, Kita A, Shimizu Y, Shuntoh H, Sio SO, Kuno T. 2003. Feedback regulation of MAPK signalling by an RNA-binding protein. Nature 424:961-96.
6. Sugiura R, Kita A, Kuno T. 2004. Upregulation of mRNA in MAPK signaling - Transcriptional activation or mRNA stabilization? Cell Cycle 3:286-288.
7. Perez P, Cansado J. 2010. Cell integrity signaling and response to stress in fission yeast. Curr Protein Pept Sci 11:680-692.

8. Satoh R, Matsumura Y, Tanaka A, Takada M, Ito Y, Hagihara K, Inari M, Kita A, Fukao A, Fujiwara T, Hirai S, Tani T, Sugiura R. 2017. Spatial regulation of the KH domain RNA-binding protein Rnc1 mediated by a Crm1-independent nuclear export system in *Schizosaccharomyces pombe*. Mol Microbiol 104:428-448.
9. Chen D, Toone WM, Mata J, Lyne R, Burns G, Kivinen K, Brazma A, Jones N, Bahler J. 2003. Global transcriptional responses of fission yeast to environmental stress. Mol Biol Cell 14:214-229.
10. Mutavchiev DR, Leda M, Sawin KE. 2016. Remodeling of the fission yeast Cdc42 cell-polarity module via the Sty1 p38 Stress-Activated Protein Kinase Pathway. Curr Biol 26:2921-2928.
11. Rodriguez-Gabriel MA, Burns G, McDonald WH, Martin V, Yates JR, 3rd, Bahler J, Russell P. 2003. RNA-binding protein Csx1 mediates global control of gene expression in response to oxidative stress. EMBO J 22:6256-66.
12. Madrid M, Nunez A, Soto T, Vicente-Soler J, Gacto M, Cansado J. 2007. Stress-activated protein kinase-mediated down-regulation of the cell integrity pathway mitogen-activated protein kinase Pmkl by protein phosphatases. Mol Biol Cell 18:4405-4419.
13. Moreno S, Klar A, Nurse P. 1991. Molecular genetic-analysis of fission yeast *Schizosaccharomyces pombe*. Methods Enzymol 194:795-823.
14. Sugiura R, Toda T, Shuntoh H, Yanagida M, Kuno T. 1998. *pmp1+*, a suppressor of calcineurin deficiency, encodes a novel MAP kinase phosphatase in fission yeast. EMBO J 17:140-148.
15. Petersen J, Hagan IM. 2005. Polo kinase links the stress pathway to cell cycle control and tip growth in fission yeast. Nature 435:507-512.
16. Lopez-Aviles S, Grande M, Gonzalez M, Helgesen AL, Alemany V, Sanchez-Piris M, Bachs O, Millar JB, Aligue R. 2005. Inactivation of the Cdc25 phosphatase by the stress-activated Srk1 kinase in fission yeast. Mol Cell 17:49-59.
17. Morigasaki S, Ikner A, Tatebe H, Shiozaki K. 2013. Response regulator-mediated MAPKKK heteromer promotes stress signaling to the Spc1 MAPK in fission yeast. Mol Biol Cell 24:1083-1092.
18. Shiozaki K, Shiozaki M, Russell P. 1998. Heat stress activates fission yeast Spc1/StyI MAPK by a MEKK-independent mechanism. Mol Biol Cell 9:1339-1349.
19. Rodriguez-Gabriel MA, Russell P. 2005. Distinct signaling pathways respond to arsenite and reactive oxygen species in *Schizosaccharomyces pombe*. Eukaryot Cell 4:1396-1402.
20. Chatterji P, Rustgi AK. 2018. RNA binding proteins in intestinal epithelial biology and colorectal cancer. Trends Mol Med 24:490-506.
21. Madrid M, Soto T, Franco A, Paredes V, Vicente J, Hidalgo E, Gacto M, Cansado J. 2004. A cooperative role for Atf1 and Pap1 in the detoxification of the oxidative stress induced by glucose deprivation in *Schizosaccharomyces pombe*. J Biol Chem 279:41594-41602.
22. Quinn J, Findlay VJ, Dawson K, Millar JB, Jones N, Morgan BA, Toone WM. 2002. Distinct regulatory proteins control the graded transcriptional response to increasing H(2)O(2) levels in fission yeast *Schizosaccharomyces pombe*. Mol Biol Cell 13:805-816.

23. Garcia-Maurino SM, Rivero-Rodriguez F, Velazquez-Cruz A, Hernandez-Vellisca M, Diaz-Quintana A, De la Rosa MA, Diaz-Moreno I. 2017. RNA Binding protein regulation and cross-talk in the control of AU-rich mRNA fate. Front Mol Biosci 4:71.
24. Lee EK. 2012. Post-translational modifications of RNA-binding proteins and their roles in RNA granules. Curr Protein Pept Sci 13:331-336.
25. Salgado A, Lopez-Serrano Oliver A, Matia-Gonzalez AM, Sotelo J, Zarco-Fernandez S, Munoz-Olivas R, Camara C, Rodriguez-Gabriel MA. 2012. Response to arsenate treatment in *Schizosaccharomyces pombe* and the role of its arsenate reductase activity. PLoS One 7:e43208.
26. Madrid M, Soto T, Khong H, Franco A, Vicente J, Perez P, Gacto M, Cansado J. 2006. Stress-induced response, localization, and regulation of the Pmk1 cell integrity pathway in *Schizosaccharomyces pombe*. J Biol Chem 281:2033-2043.
27. Jarvelin AI, Noerenberg M, Davis I, Castello A. 2016. The new (dis)order in RNA regulation. Cell Commun Signal 14:9.
28. Teplova M, Malinina L, Darnell JC, Song J, Lu M, Abagyan R, Musunuru K, Teplov A, Burley SK, Darnell RB, Patel DJ. 2011. Protein-RNA and protein-protein recognition by dual KH1/2 domains of the neuronal splicing factor Nova-1. Structure 19:930-944.
29. Bahler J, Wu J, Longtine M, Shah N, McKenzie A, Steever A, Wach A, Philippsen P, Pringle J. 1998. Heterologous modules for efficient and versatile PCR-based gene targeting in *Schizosaccharomyces pombe*. Yeast 14:943-951.
30. Zheng L, Baumann U, Reymond JL. 2004. An efficient one-step site-directed and site-saturation mutagenesis protocol. Nucleic Acids Res 32:e115.
31. Guan K, Dixon J. 1991. Eukaryotic proteins expressed in *Escherichia coli* - an improved thrombin cleavage and purification procedure of fusion proteins with glutathione-S-transferase. Anal Biochem 192:262-267.
32. Madrid M, Jimenez R, Sanchez-Mir L, Soto T, Franco A, Vicente-Soler J, Gacto M, Perez P, Cansado J. 2015. Multiple layers of regulation influence cell integrity control by the PKC ortholog Pck2 in fission yeast. J Cell Sci 128:266-80.
33. Grallert A, Hagan IM. 2017. Preparation of prote in extracts from *Schizosaccharomyces pombe* using trichloroacetic acid precipitation. Cold Spring Harb Protoc 2017(2). doi: 10.1101/pdb.prot091579.
34. Navarro FJ, Chakravarty P, Nurse P. 2017. Phosphorylation of the RNA-binding protein Zfs1 modulates sexual differentiation in fission yeast. J Cell Sci 130:4144-4154.
35. Schneider C, Rasband W, Eliceiri K. 2012. NIH Image to ImageJ: 25 years of image analysis. Nat Methods 9:671-675.

FIGURE LEGENDS

FIG 1

(A) The *S. pombe* stress activated (SAPK) and cell integrity (CIP) MAP kinase pathways. Please see text for a detailed description of their main components and functions. (B) Cell length at division of *S. pombe* cells growing exponentially in YES medium are presented as scatter plots showing the average values ± SD (number of independent biological replicates=3) for the wild type and mutant strains of the indicated genotypes (number of cells ≥ 200/strain). Significant differences were assessed by Turkey's test following one-way ANOVA for the comparisons with respective values of wild-type cells. ****, $P<0.0001$; ns, not significant. Cell morphology of each strain was analyzed by fluorescence microscopy after staining with Calcofluor white. Scale bar: 10 μm. (C) *cdc25-22* (control) and *cdc25-22 rnc1*Δ *S. pombe* cultures were incubated in YES medium at the restrictive temperature (36.5ºC) for 3.5h, and cell length at G2 was measured and represented as scatter plots showing the average values ± SD for three independent biological replicates (number of cells ≥ 200/strain). Significant differences were assessed by Turkey's test following one-way ANOVA for the comparisons with respective values of wild-type cells. ****, $P<0.0001$. Cell morphology of each strain was analyzed by fluorescence microscopy after staining with Calcofluor white. Scale bar: 10 μm. (D) *S. pombe* wild type, *pmk1*Δ, and *rnc1*Δ cells expressing a genomic Sty1-HA6his fusion were grown in YES medium to mid-log phase. Activated/total Sty1 were detected with anti-phospho-p38 and anti-HA antibodies, respectively. Relative units as mean ± SD (biological triplicates) for Sty1 phosphorylation (anti-phospho-p38 blot) were determined with respect to the internal control (anti-HA blot). ***, $P<0.005$;* ns, not significant, as calculated by unpaired Student´s *t* test.

FIG 2

(A) mRNA levels of the indicated genes were measured by qPCR from total RNA extracted from cell samples corresponding to *S. pombe* wild type and *rnc1*Δ strains growing exponentially in YES medium. Results are shown as relative fold expression (mean ± SD) from three biological repeats. *, $P<0.05$; ns, not significant, as calculated by unpaired Student´s *t* test. (B) Upper panel: Total extracts from growing cultures of wild type and *rnc1*Δ strains or those expressing Mcs4-GFP, Wak1-13myc, Wis1-13myc, Sty1-HA, Pyp1-13myc, Pyp2-13myc, and Ptc1-13myc genomic fusions were resolved by SDS-PAGE, and the levels of the respective proteins were detected by incubation with anti-Atf1, anti-HA, anti-GFP, and anti-c-myc antibodies. Anti-Cdc2 was used as a loading control. Lower panel: quantification of Western blot experiments. **, P<0.05;* ns, not significant, as calculated by unpaired Student´s *t* test. (C) *S. pombe* wild type, *pyp1*Δ, *rnc1*Δ, and *pyp1*Δ *rnc1*Δ cells expressing a genomic Sty1-HA6his fusion were grown in YES medium to mid-log phase. Activated/total Sty1 were detected with anti-phospho-p38 and anti-HA antibodies, respectively. Total levels of Atf1 and Pyp2-13myc fusion were determined as described in (B).

FIG 3

(A) mRNA levels of the indicated genes were measured by qPCR from total RNA extracted from cell samples corresponding to *S. pombe* wild type and *rnc1*Δ strains growing exponentially in YES medium and treated with 0.6M KCl for the indicated times. Results are shown as relative fold expression (mean ± SD) from three biological repeats. *, $P<0.05$; ns, not significant, for the comparisons of *rnc1*Δ cells with the corresponding incubation times of wild-type cells as calculated by unpaired Student´s *t* test. (B) *S. pombe* wild type and *rnc1*Δ cells expressing a genomic Sty1-HA6his fusion were grown in YES medium to mid-

log phase, and treated with either 0.6 M KCl for the indicated times. Activated/total Sty1 were detected with anti-phospho-p38 and anti-HA antibodies, respectively. Relative units as mean ± SD (biological triplicates) for Sty1 phosphorylation (anti-phospho-p38 blot) were determined with respect to the internal control (anti-HA blot). **, P<0.05;* as calculated by unpaired Student´s *t* test. (C) and (D) *S. pombe* wild type and *rnc1*Δ cells expressing either genomic Wak1-13myc or Wis1-13myc fusions were grown in YES medium to mid-log phase, treated with 0.6 M KCl for the indicated times, and total levels of Wak1-13myc and Wis1-13myc were detected by incubation with anti-c-myc antibodies. Anti-Cdc2 was used as a loading control. **, P<0.05;* as calculated by unpaired Student´s *t* test. (E) Total extracts from growing cultures of wild type and *rnc1*Δ strains or those expressing Pyp1-13myc or Pyp2-13myc genomic fusions and treated with either 0.6 M KCl for the indicated times, were resolved by SDS-PAGE, and the levels of the respective proteins were detected by incubation with anti-Atf1 and anti-c-myc antibodies. Anti-Cdc2 was used as a loading control. **, P<0.05;* as calculated by unpaired Student´s *t* test. (F) *S. pombe* wild type and *rnc1*Δ cells expressing a genomic Pmk1-HA6his fusion were grown in YES medium to mid-log phase, and treated with either 0.6 M KCl for the indicated times. Activated/total Pmk1 were detected with anti-phospho-p44/42 and anti-HA antibodies, respectively. ***, P<0.005;* ns, not significant, as calculated by unpaired Student´s *t* test.

FIG 4

(A) Secondary structure of Rnc1. KH domains appear colored in light blue. Putative S/T MAPK-phospho sites are shown. Prediction of intrinsically disordered regions (light green boxes) with IUpred2 (https://iupred2a.elte.hu/) is shown below. (B) Co-immunoprecipitation of Rnc1-3HA and Sty-GFP genomic fusions from yeast extracts obtained from vegetatively growing cultures of the indicated genotypes. Results from a representative experiment are

shown. (C) Bacterially purified GST-Rnc1, GST-Rnc1(T50A), or GST-Rnc1(S/T56A) fusions were incubated with ATP-γ-S and GST-Wis1DD (constitutively active MAPKK) and GST-Sty1-(T97A) (analog-sensitive MAP kinase), in the presence or absence of an specific kinase inhibitor (3-Br-PP1). Rnc1 thiophosphorylation was detected with anti-thioP-ester antibody. Total Wis1, Sty1 and Rnc1 levels in the reaction were determined after incubation with anti-GST antibody. Results from a representative experiment are shown. (D) *S. pombe* cells expressing Rnc1-3HA or Rnc1(S/T6A)-3HA genomic fusions were grown in YES medium with 7% glucose, recovered by filtration, and resuspended in the same medium lacking glucose and osmotically equilibrated with 3% glycerol for the indicated times. Total and phosphorylated Rnc1 levels were by immunobloting of TCA-precipitated protein extracts with anti-HA antibody. Anti-Cdc2 was used as a loading control. Results from a representative experiment are shown. P-species: Rnc1-phosphorylated species.
(E) Extracts from *S. pombe* growing cells starved from glucose for 60 min and expressing a genomic Rnc1-3HA fusion were treated with lambda phosphatase in the presence/absence of specific phosphatase inhibitor. Total and phosphorylated Rnc1 levels were determined by immunobloting with anti-HA antibody. Anti-Cdc2 was used as a loading control. Results from a representative experiment are shown. (F) *cdc10-129* (G1-phase arrest), *cdc25-22* (G2-phase arrest), and *nda3-km311* (M-phase arrest) mutants expressing a genomic Rnc1-3HA fusion were incubated at either 36.5ºC for 3.5 h (*cdc10-129* and *cdc25-22* backgrounds) or 18 ºC for 7h (*nda3-km311* background). Total and phosphorylated Rnc1 levels were determined by immunobloting with anti-HA antibody. Anti-Cdc2 was used as a loading control. Results from a representative experiment are shown. (G) Cells from *cdc25-22* and *cdc25-22 pmk1Δ* strains expressing a genomic Rnc1-3HA fusion were grown to an A_{600} of 0.3 at 25ºC, shifted to 37ºC for 3.5 h, and then released from the growth arrest by transfer back to 25ºC. Aliquots were taken at the indicated time intervals and Rnc1, Cdc2

phosphorylation at Y15 or total Cdc2 were detected by immunoblotting with anti-HA, anti-Cdc2 pY15 and anti-Cdk1/Cdc2 (PSTAIR) antibodies, respectively. Right panel shows the corresponding percentages of binucleated and septated cells. Results from representative experiments are shown. (H) Wild type, *pmk1Δ, sty1Δ*, and *sty1Δ pmk1Δ* strains expressing a Rnc1-3HA genomic fusion were grown in YES medium, and resuspended in the same medium lacking glucose and osmotically equilibrated with 3% glycerol (upper panel), incubated at 40ºC (middle panel), or treated with 0.5 mM sodium arsenite (lower panel) for the indicated times. Total and phosphorylated Rnc1 levels were determined by immunobloting of TCA-precipitated protein extracts with anti-HA antibody. Anti-Cdc2 was used as a loading control. Results from representative experiments are shown.

FIG 5

(A) GST, GST-Rnc1, GST-Rnc1(mKH) and GST-Rnc1(S/T6A) fusions purified from *S. pombe* cultures were separately incubated with total RNA, and, after extensive washes, the RNA binding ability of Rnc1with respect to the indicated transcripts was measured by RT-qPCR and normalized with *leu*+ mRNA. (B) mRNA levels of the indicated genes were measured by qPCR from total RNA extracted from cell samples corresponding to *S. pombe* cells growing exponentially in YES medium and expressing either Rnc1-3HA (wild type), Rnc1-(mKH)-3HA, or Rnc1-(S/T6A)-3HA genomic fusions. Results are shown as relative fold expression (mean $\pm$ SD) from three biological repeats. *, $P<0.05$; ns, not significant, as calculated by unpaired Student´s *t* test. (C) Left: Total extracts from growing cultures of strains co-expressing either Rnc1-3HA (wild type), Rnc1-(mKH)-3HA, or Rnc1-(S/T6A)-3HA with Wak1-13myc, Wis1-13myc, Pyp1-13myc, or Pyp2-13myc genomic fusions were resolved by SDS-PAGE, and the levels of the indicated proteins were detected by incubation with anti-Atf1 and anti-c-myc antibodies. Anti-Cdc2 was used as a loading

control. Right: quantification of Western blot experiments. **, P<0.05;* ns, not significant, as calculated by unpaired Student´s *t* test. (D) Rnc1-3HA (wild type), Rnc1-(mKH)-3HA, and Rnc1-(S/T6A)-3HA cells expressing genomic Sty1-HA6his fusions were grown in YES medium to mid-log phase. Activated/total Sty1 were detected with anti-phospho-p38 and anti-HA antibodies, respectively. Relative units as mean ± SD (biological triplicates) for Sty1 phosphorylation (anti-phospho-p38 blot) were determined with respect to the internal control (anti-HA blot). **, P<0.05;* as calculated by unpaired Student´s *t* test. (E) Cell length at division of *S. pombe* Rnc1-3HA (wild type), Rnc1-(mKH)-3HA, and Rnc1-(S/T6A)-3HA cells growing exponentially in YES medium are presented as scatter plots showing the average values ± SD (number of independent biological replicates=3; number of cells ≥ 200/strain). Significant differences were assessed by Turkey's test following one-way ANOVA for the comparisons with respective values of wild-type cells. *, *P*<0.05. Cell morphology of each strain was analyzed by fluorescence microscopy after staining with Calcofluor white. Scale bar: 10μm.

FIG 6

(A) Total extracts from growing cultures of Rnc1-3HA (wild type), Rnc1-(mKH)-3HA, and Rnc1-(S/T6A)-3HA cells growing exponentially and expressing either Wak1-13myc, Wis1-13myc, Sty1-HA6his, Pyp1-13myc, Pyp2-13myc or Pmk1-HA6his genomic fusions were treated with 0.6 M KCl for the indicated times. Total levels of Wak1, Wis1, Atf1, Pyp1, and Pyp2 were detected by incubation with anti-Atf1 and anti-c-myc antibodies. Anti-Cdc2 was used as a loading control. Activated/total Sty1 were detected with anti-phospho-p38 and anti-HA antibodies, respectively. Activated/total Pmk1 were detected with anti-phospho-p44/42 and anti-HA antibodies, respectively. Results from representative experiments are shown. (B) Percentage of decay in the expression levels of *wak1+*,*wis1+*, *pyp1+*, and

pyp2+ mRNAs with respect to 28S RNA (no decay during the experiment) were measured by qPCR from *S. pombe* cultures expressing either Rnc1-3HA (wild type), Rnc1-(mKH)-3HA, or Rnc1-(S/T6A)-3HA genomic fusions, and treated for the indicated times with 1,10-phenantroline to block transcription. Results are shown as relative fold expression (mean ± SD) from three biological repeats. *, $P<0.05$; ns, not significant, as calculated by unpaired Student´s *t* test. (C) Decimal dilutions of strains of the indicated genotypes were spotted on YES solid plates and incubated in an oven at 55ºC for the indicated times. The plates were then removed from the oven, incubated at 30ºC for 3 days, and photographed. Representative experiments are shown. (D) Cross-regulatory interactions between Rnc1 and the stress activated MAPK signaling pathway (SAPK) in fission yeast. For specific details please see text.

SUPPLEMENTARY FIGURES LEGENDS

Fig. S1

S. pombe wild type, *sty1*Δ, and *rnc1*Δ cells expressing a genomic Pmk1-HA6his fusion were grown in YES medium to mid-log phase. Activated/total Pmk1 were detected with anti-phospho-p44/42 and anti-HA antibodies, respectively. Relative units as mean ± SD (biological triplicates) for Pmk1 phosphorylation (anti-phospho-p44/42 blot) were determined with respect to the internal control (anti-HA blot). ***, P<0.005;* ns, not significant, as calculated by unpaired Student´s *t* test.

Fig. S2

(A) Cell length at division of *S. pombe* wild type and Rnc1-3HA cells growing exponentially in YES medium showing the average values ± SD (number of independent biological replicates=3). Cell morphology of each strain was analyzed by fluorescence microscopy after staining with Calcofluor white. Scale bar: 10μm.

(B) *S. pombe* wild type and Rnc1-3HA cells expressing genomic Sty1-HA6his fusions were grown in YES medium to mid-log phase. Activated/total Sty1 were detected with anti-phospho-p38 and anti-HA antibodies, respectively. Relative units as mean ± SD (biological triplicates) for Sty1 phosphorylation (anti-phospho-p38 blot) were determined with respect to the internal control (anti-HA blot). ***, P<0.005,* as calculated by unpaired Student´s *t* test.

Fig. S3

Decimal dilutions of strains of the indicated genotypes were spotted on YES solid plates with the indicated compounds, incubated at either 28 or 36ºC for 3 days, and then photographed. Representative experiments are shown.

Fig. S4

UCAU motifs present at the 3´UTRs sequences corresponding to *wak1+, wis1+, atf1+, pyp1+* and *pyp2+* mRNAs are marked in yellow.

Table S1. *S. pombe* strains used in this study.

Table S2. Oligonucleotides and DNA fragments used in this study.

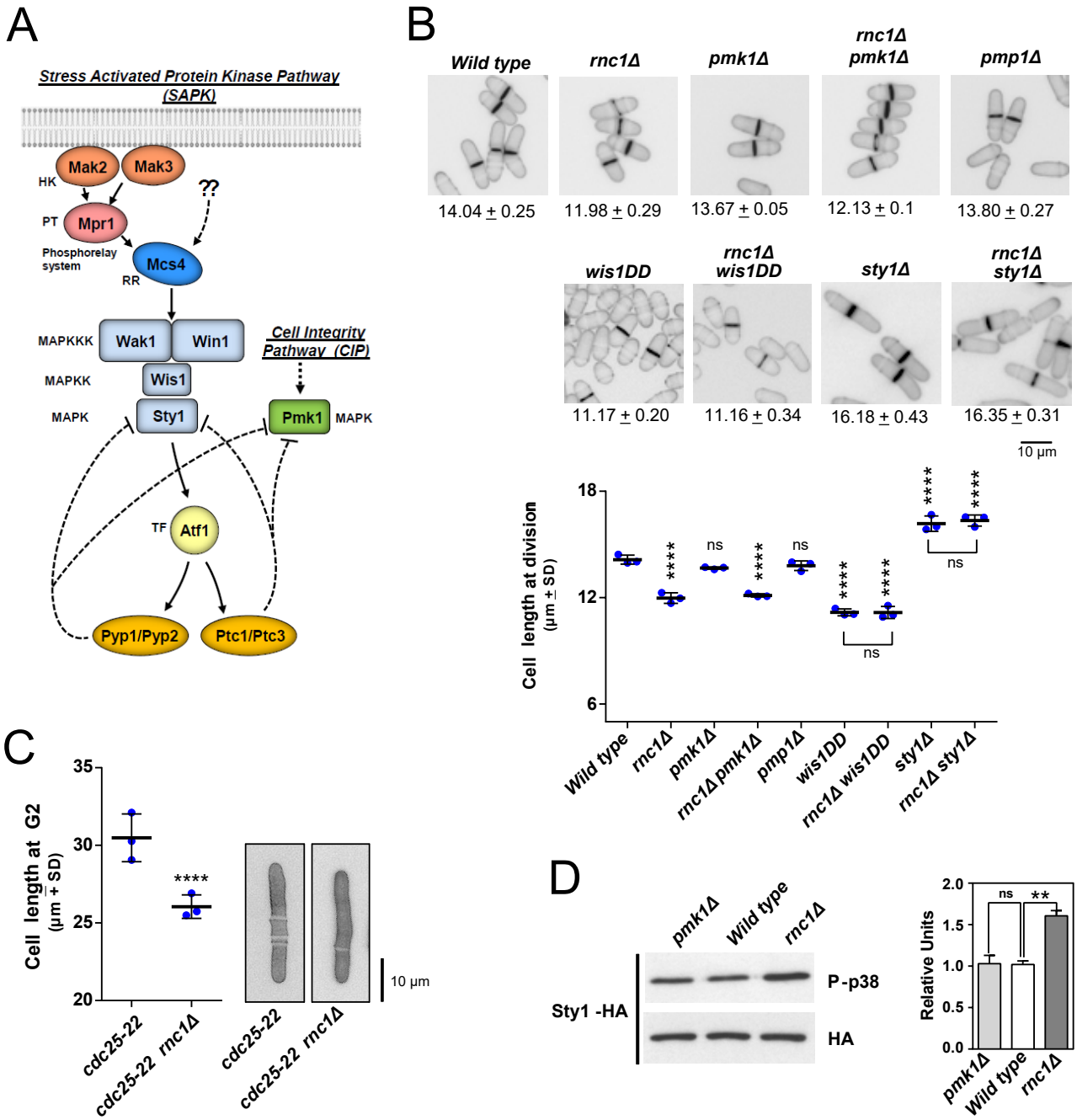
A
Stress Activated Protein Kinase Pathway (SAPK)
Mak2
Mak3
HK
??
PT
Mpr1
Phosphorelay system
Mcs4
RR
MAPKKK
Wak1
Win1
Cell Integrity Pathway (CIP)
MAPKK
Wis1
MAPK
Sty1
Pmk1
MAPK
TF
Atf1
Pyp1/Pyp2
Ptc1/Ptc3
B
Wild type
rnc1Δ
pmk1Δ
rnc1Δ pmk1Δ
pmp1Δ
14.04 ± 0.25
11.98 ± 0.29
13.67 ± 0.05
12.13 ± 0.1
13.80 ± 0.27
wis1DD
rnc1Δ wis1DD
sty1Δ
rnc1Δ sty1Δ
11.17 ± 0.20
11.16 ± 0.34
16.18 ± 0.43
16.35 ± 0.31
10 µm
Cell length at division (µm ± SD)
18
12
6
****
ns
Wild type
rnc1Δ
pmk1Δ
rnc1Δ pmk1Δ
pmp1Δ
wis1DD
rnc1Δ wis1DD
sty1Δ
rnc1Δ sty1Δ
C
Cell length at G2 (µm ± SD)
35
30
25
20
****
cdc25-22
cdc25-22 rnc1Δ
10 µm
D
pmk1Δ
Wild type
rnc1Δ
Sty1 -HA
P-p38
HA
Relative Units
2.0
1.5
1.0
0.5
0.0
ns
**

Fig. 1

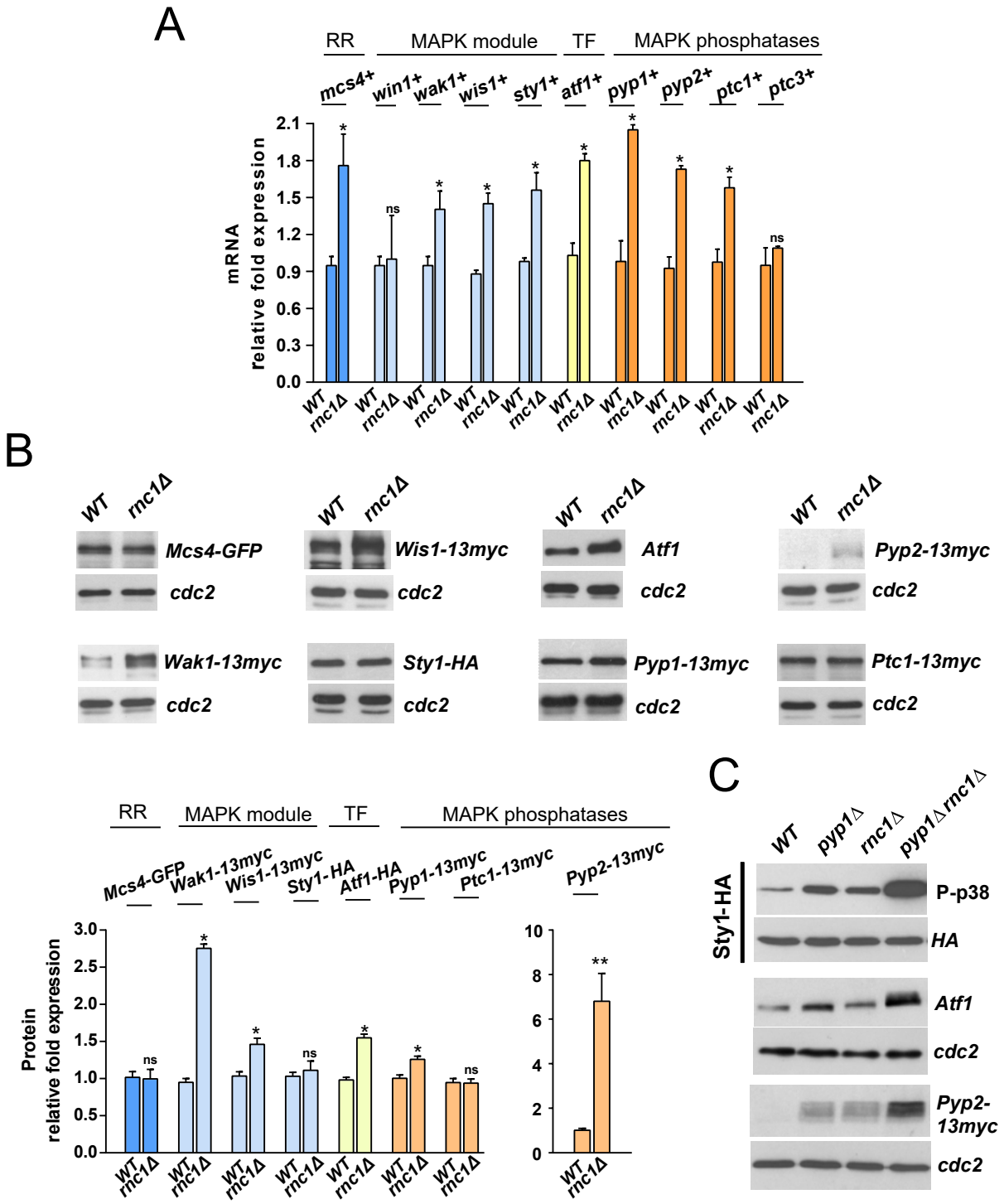
A
RR
MAPK module
TF
MAPK phosphatases
mcs4+
win1+
wak1+
wis1+
sty1+
atf1+
pyp1+
pyp2+
ptc1+
ptc3+
mRNA relative fold expression
2.1
1.8
1.5
1.2
0.9
0.6
0.3
0.0
ns
WT
rnc1Δ
B
Mcs4-GFP
cdc2
Wis1-13myc
Atf1
Pyp2-13myc
Wak1-13myc
Sty1-HA
Pyp1-13myc
Ptc1-13myc
Protein relative fold expression
3.0
2.5
2.0
1.5
1.0
0.5
0.0
10
8
6
4
2
0
**
C
pyp1Δ
rnc1Δ
pyp1Δrnc1Δ
Sty1-HA
P-p38
HA
Atf1
Pyp2-13myc

Fig. 2

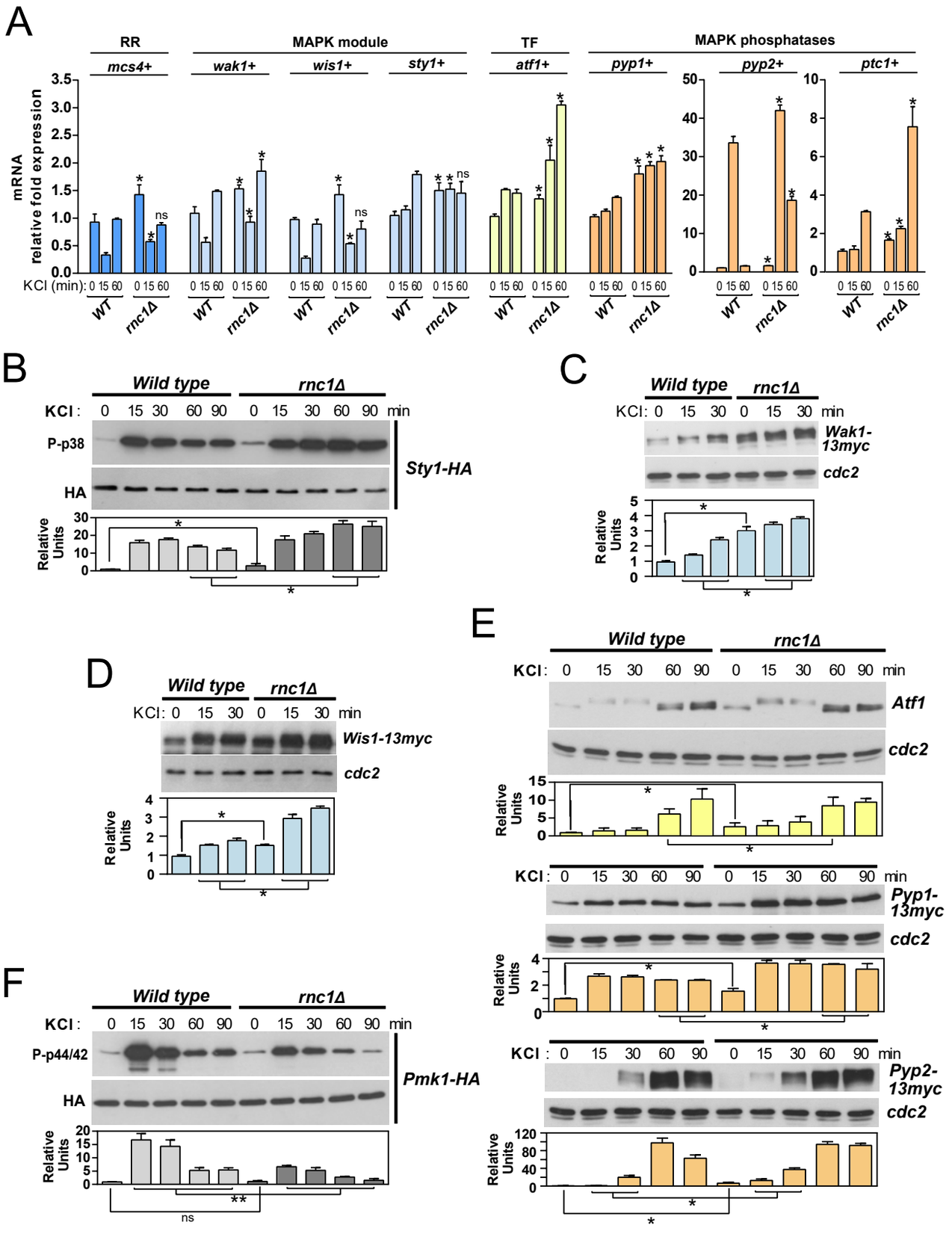
A
RR
MAPK module
TF
MAPK phosphatases
mcs4+
wak1+
wis1+
sty1+
atf1+
pyp1+
pyp2+
ptc1+
mRNA relative fold expression
KCl (min): 0 15 60
WT
rnc1Δ
B
Wild type
rnc1Δ
KCl : 0 15 30 60 90 0 15 30 60 90 min
P-p38
HA
Sty1-HA
Relative Units
C
Wild type
rnc1Δ
KCl: 0 15 30 0 15 30 min
Wak1-13myc
cdc2
Relative Units
D
Wild type
rnc1Δ
KCl: 0 15 30 0 15 30 min
Wis1-13myc
cdc2
Relative Units
E
Wild type
rnc1Δ
KCl : 0 15 30 60 90 0 15 30 60 90 min
Atf1
cdc2
Relative Units
Pyp1-13myc
Pyp2-13myc
F
Wild type
rnc1Δ
KCl : 0 15 30 60 90 0 15 30 60 90 min
P-p44/42
HA
Pmk1-HA
Relative Units
ns

Fig. 3

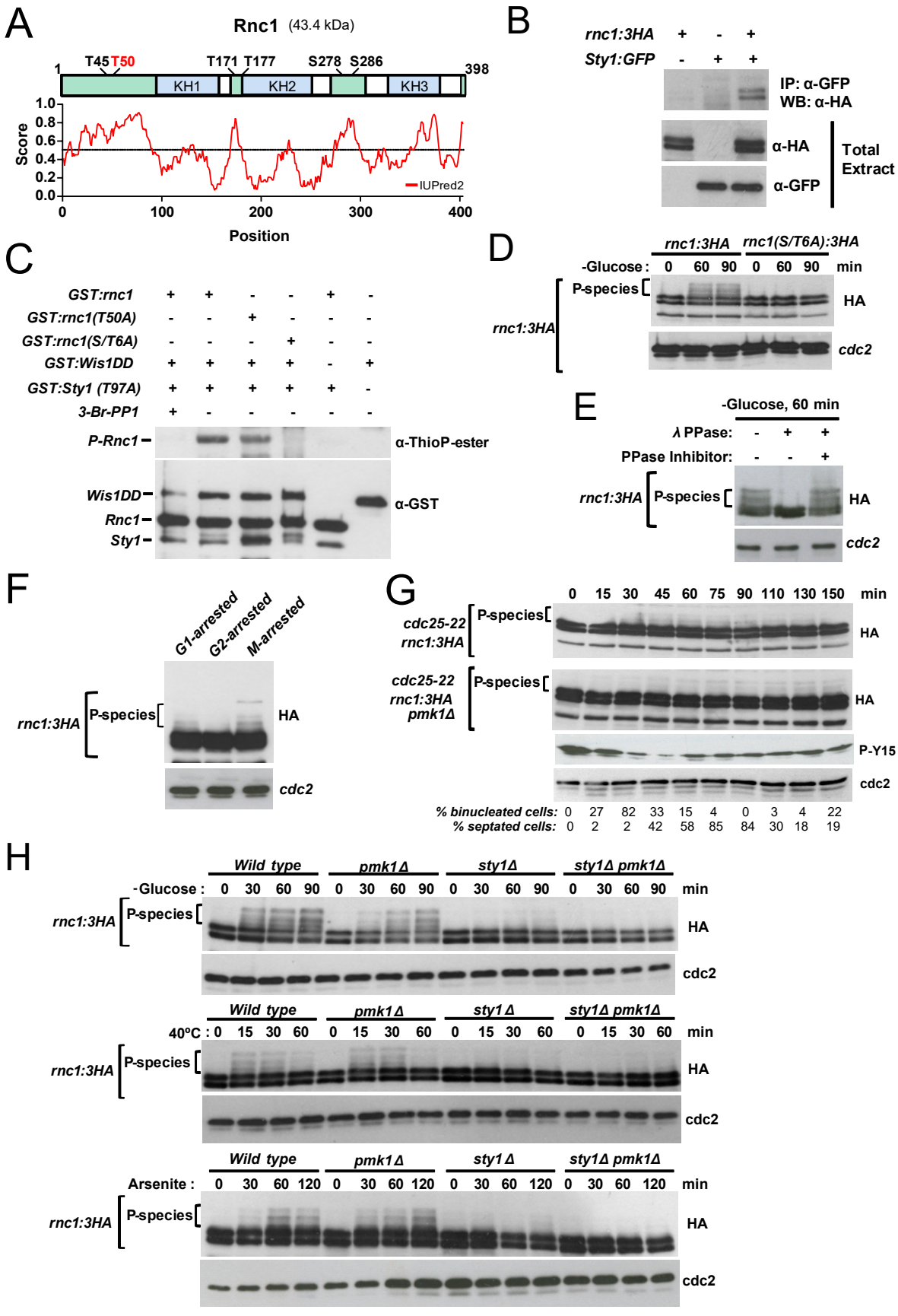
A
Rnc1 (43.4 kDa)
T45 T50
T171 T177
S278 S286
1
398
KH1
KH2
KH3
Score
IUPred2
Position
B
rnc1:3HA
Sty1:GFP
IP: α-GFP
WB: α-HA
α-HA
α-GFP
Total Extract
C
GST:rnc1
GST:rnc1(T50A)
GST:rnc1(S/T6A)
GST:Wis1DD
GST:Sty1 (T97A)
3-Br-PP1
P-Rnc1
α-ThioP-ester
Wis1DD
Rnc1
Sty1
α-GST
D
rnc1:3HA
rnc1(S/T6A):3HA
-Glucose :
min
P-species
HA
cdc2
E
-Glucose, 60 min
λ PPase:
PPase Inhibitor:
F
G1-arrested
G2-arrested
M-arrested
G
cdc25-22
pmk1Δ
P-Y15
% binucleated cells:
% septated cells:
H
Wild type
pmk1Δ
sty1Δ
sty1Δ pmk1Δ
40°C :
Arsenite :

Fig. 4

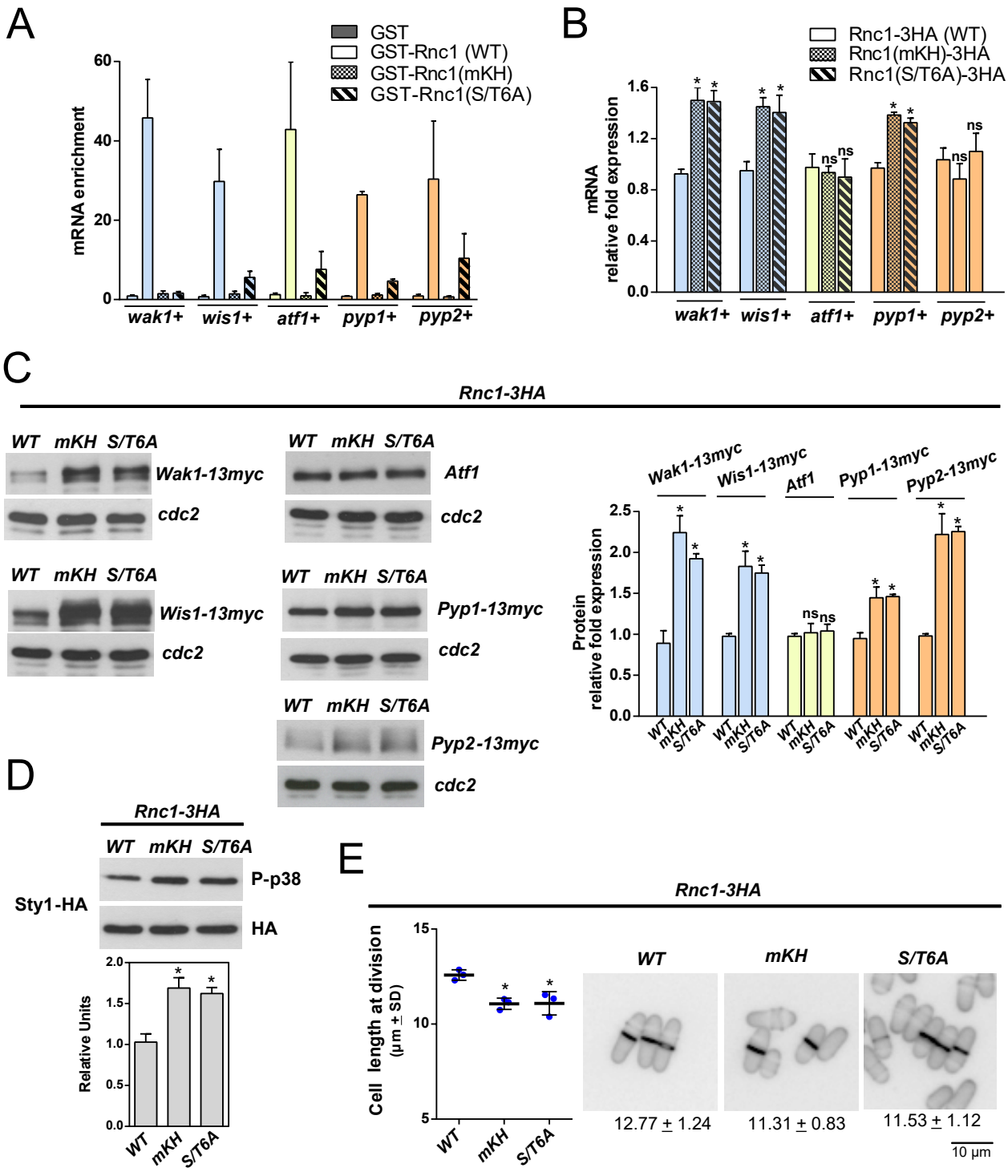
A
GST
GST-Rnc1 (WT)
GST-Rnc1(mKH)
GST-Rnc1(S/T6A)
mRNA enrichment
60
40
20
0
wak1+
wis1+
atf1+
pyp1+
pyp2+
B
Rnc1-3HA (WT)
Rnc1(mKH)-3HA
Rnc1(S/T6A)-3HA
mRNA relative fold expression
1.6
1.2
0.8
0.4
0.0
ns
C
Rnc1-3HA
WT mKH S/T6A
Wak1-13myc
cdc2
Atf1
Wis1-13myc
Pyp1-13myc
Pyp2-13myc
Protein relative fold expression
2.5
2.0
1.5
1.0
0.5
0.0
D
Rnc1-3HA
Sty1-HA
P-p38
HA
Relative Units
2.0
1.5
1.0
0.5
0.0
E
Rnc1-3HA
Cell length at division (µm ± SD)
15
10
5
WT
mKH
S/T6A
12.77 ± 1.24
11.31 ± 0.83
11.53 ± 1.12
10 µm

Fig. 5

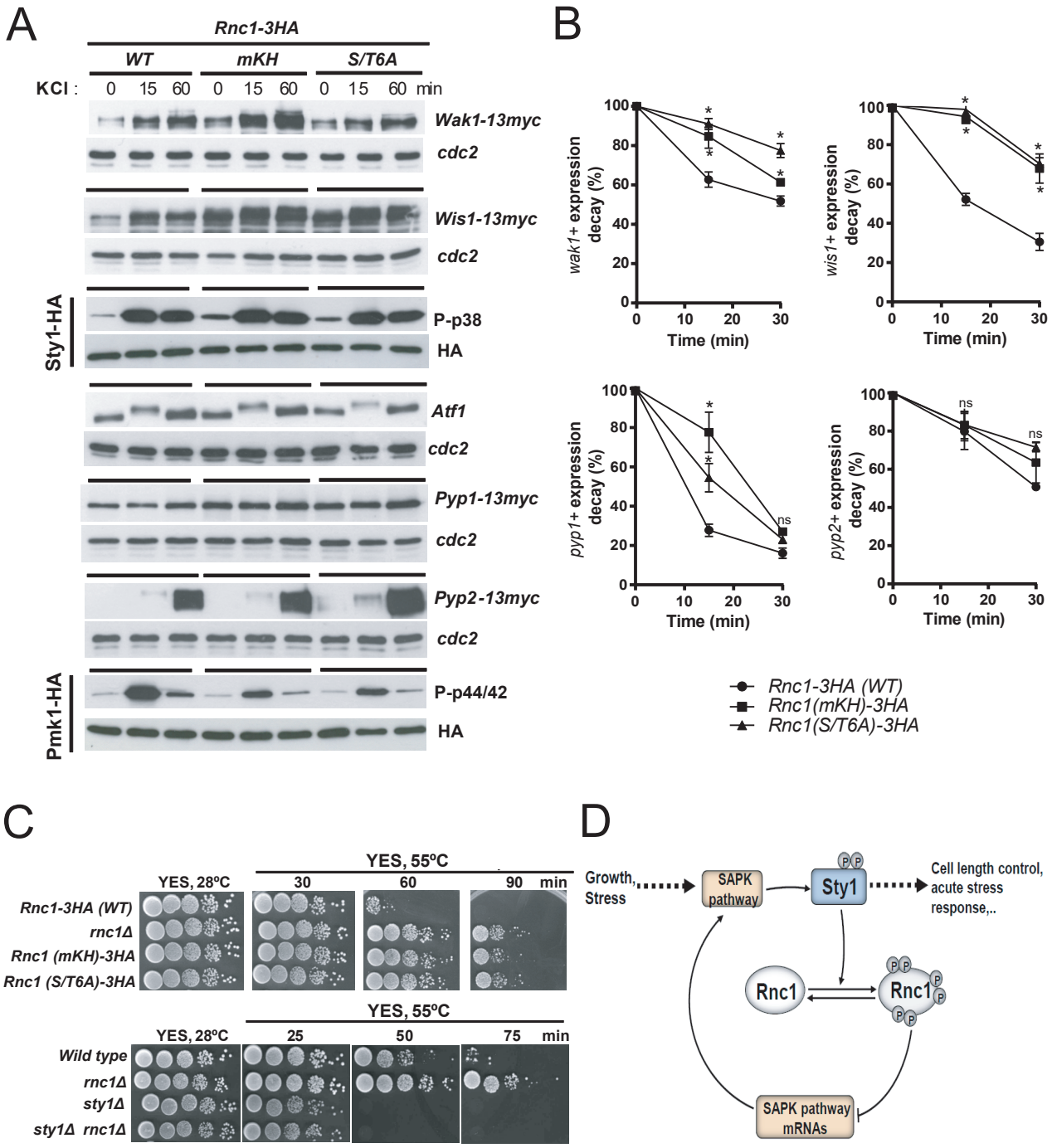
A
Rnc1-3HA
WT
mKH
S/T6A
KCl : 0 15 60 0 15 60 0 15 60 min
Wak1-13myc
cdc2
Wis1-13myc
cdc2
Sty1-HA
P-p38
HA
Atf1
cdc2
Pyp1-13myc
cdc2
Pyp2-13myc
cdc2
Pmk1-HA
P-p44/42
HA
B
wak1+ expression decay (%)
wis1+ expression decay (%)
pyp1+ expression decay (%)
pyp2+ expression decay (%)
Time (min)
ns
Rnc1-3HA (WT)
Rnc1(mKH)-3HA
Rnc1(S/T6A)-3HA
C
YES, 28ºC
YES, 55ºC
30
60
90 min
Rnc1-3HA (WT)
rnc1Δ
Rnc1 (mKH)-3HA
Rnc1 (S/T6A)-3HA
YES, 28ºC
YES, 55ºC
25
50
75 min
Wild type
rnc1Δ
sty1Δ
sty1Δ rnc1Δ
D
Growth, Stress
SAPK pathway
Sty1
Cell length control, acute stress response,..
Rnc1
Rnc1
SAPK pathway mRNAs

Fig. 6

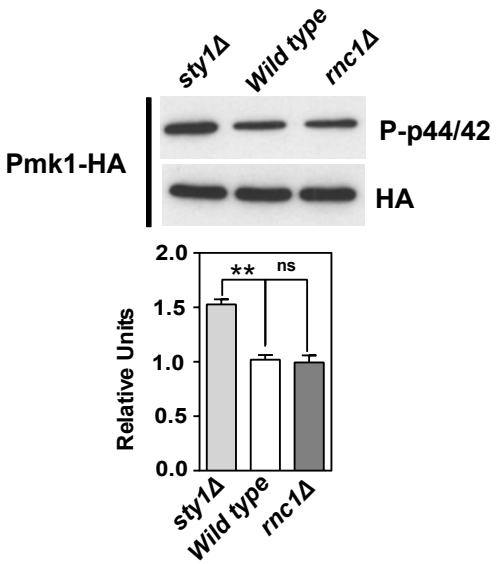

Fig. S1

S. pombe wild type, *sty1*Δ, and *rnc1*Δ cells expressing a genomic Pmk1-HA6his fusion were grown in YES medium to mid-log phase. Activated/total Pmk1 were detected with anti-phospho-p44/42 and anti-HA antibodies, respectively. Relative units as mean ± SD (biological triplicates) for Pmk1 phosphorylation (anti-phospho-p44/42 blot) were determined with respect to the internal control (anti-HA blot). ***, P<0.005;* ns, not significant, as calculated by unpaired Student´s *t* test.

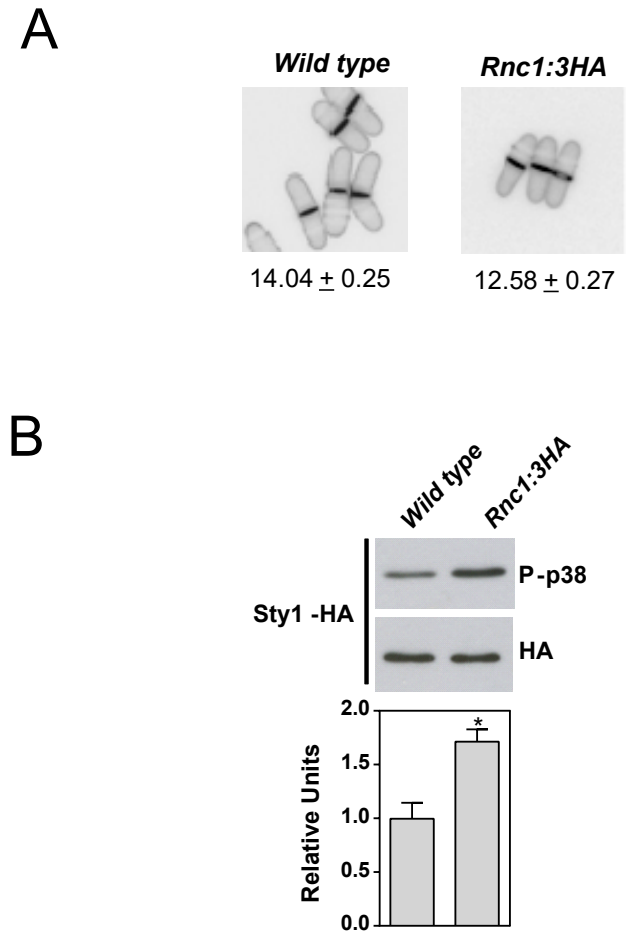

Fig. S2

(A) Cell length at division of *S. pombe* wild type and Rnc1-3HA cells growing exponentially in YES medium showing the average values ± SD (number of independent biological replicates=3). Cell morphology of each strain was analyzed by fluorescence microscopy after staining with Calcofluor white. Scale bar: 10 μm.

(B) *S. pombe* wild type and Rnc1-3HA cells expressing genomic Sty1-HA6his fusions were grown in YES medium to mid-log phase. Activated/total Sty1 were detected with anti-phospho-p38 and anti-HA antibodies, respectively. Relative units as mean ± SD (biological triplicates) for Sty1 phosphorylation (anti-phospho-p38 blot) were determined with respect to the internal control (anti-HA blot). ***, P<0.005,* as calculated by unpaired Student´s *t* test.

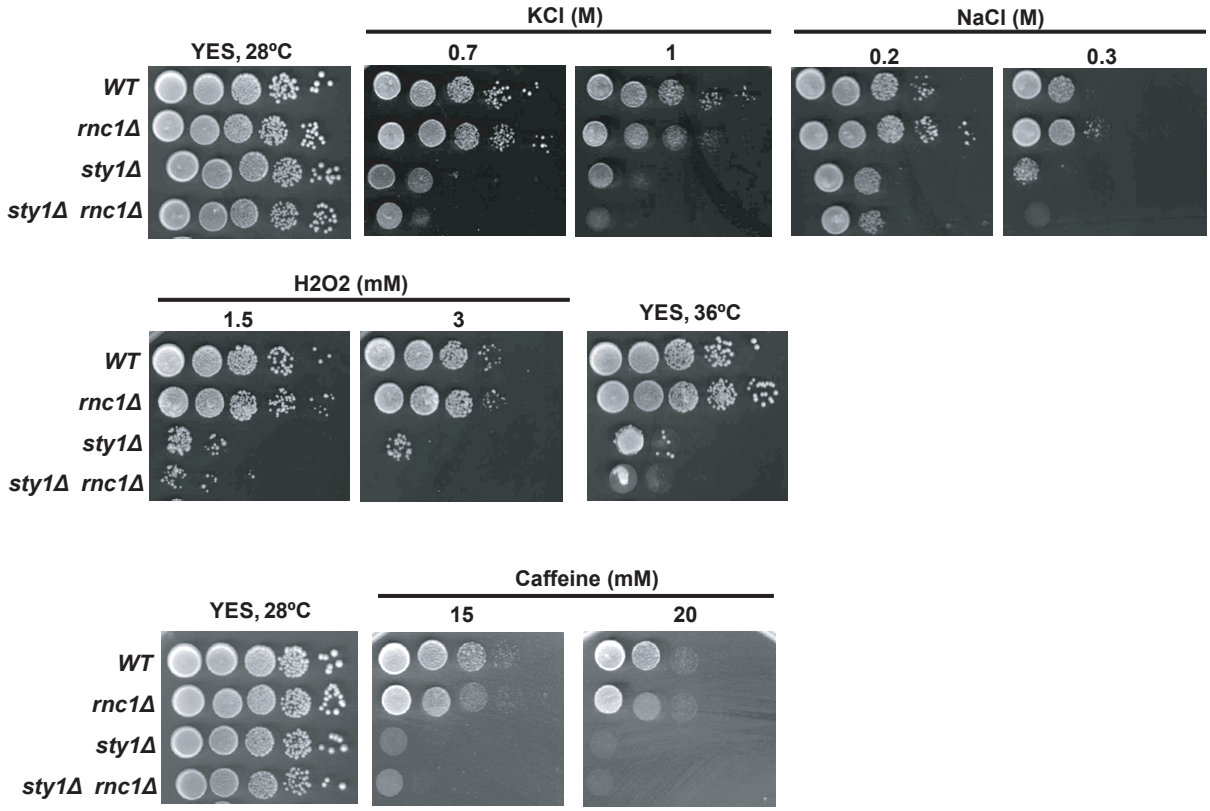

Fig. S3

Decimal dilutions of strains of the indicated genotypes were spotted on YES solid plates with the indicated compounds, incubated at either 28 or 36ºC for 3 days, and then photographed. Representative experiments are shown.

***pmp1+* 3´UTR**

CAATGCCAATTATTTATAAATACATAAAAAAAGGGAAATTTTGTCTATTCAAGTTCCGTTGTAAGTTGGT
TTTTATACTCTTCCTTATGGGTCTTAATTCTAAGCTTATCAGCTGCTTTTAAAAAATATCCACTTTATTA
TGAAGACTTACGGGTCGCTCGTCAGTTATTCATATCATTCGTCATGGACTTTTTTACAGTTTGCATTGCT
CGCTTCCAATGTATAGTTATAATTCTTGTTTAATACTTAGCTTGCAGATGTTTTATCGTTCTATGTTGCG
AATTTGTATTTACCTCAGTTTTTTACTTCTAGTCTTTGGTTCTGGGTCGGTTTGTTTACCAATGAAAAAA
ACTAGAGTTTTCATGTCATTTGTCATTGTTATTGAGTGAAATTTGTGCGTCGTGTTATTTTCTAATTCAT
TATTCTATTTTTATGCTATTTCCTTGTTATTATTACTAAACTTAATATGAGGTTGTGAATATTTATTCAA
CATCATCAGTATCTATTCTTATTCCCAGTTAAAATGATGTCCCTTCTTATCAGCAACACGGTGTCTTTAG
TTGATATAAAGCATTCCTTCAATCGTTAGAAATTTGTAAATTTCCGAGTTTACGATTCGTACTAACTTGA
GCATTCATGAATTTACAATTAAAGTTGGAAATGGTTAAATTATAAGTACATTACATTATTGCTCATAGAA
TGGACGTGTGAAAAAAAATGTTAACCCAAGCTTTAAAATCATTGCTAATAGCAAATAAAGCTAGTATTGA
AACTACTGCAAAGCTAAGATTTAAGAAATACAATAAATTTTTATTGTGTATGAACAAAAGACTGAATCTA
AGCAGCAAAGCTAGAAAGCAAAGTTTGTAAAGCAACAGAGTCCTCACCATAGTCCTAAAAAATAAGTTAG
CATGCATAGAAGAAACAATTTTCGAAAAAATGATCACATACAGTTACAGCAACACAAGAGCAGCCAACAA
CCTTACGGGCATTTCCATCACGGTCAAGAACGCACAAACCAGCCCATTCACCTAAGATCTTAGGATCAGC
TACTTTAACCAAAGGGGTTTGGGATTCAGCACAAAGGGCTTCAACAAGCTTAACATAAGCTTCTTGATCA
CAGCTCTCGCATAGAACACAAAGGTGGGCTTGGCGACGGTCAAGGGCTTTGGAAGCTTCACGGATACCGC
GAGCAAGTCCATCATGGACAAGTGCACGCTTTAGAACCTCTTTCAAAGAATCCTCAACGGACAATGGGGA
AGAACCAGTTTCCTCTTCTACAACTTCGACGGTCTCAATGACCTCTTCAGCCTGGGGCACATGATCTCCT
TCTGTTGACATTTTTAAATAATAATAAGATGCTTTTTAATCAAGACGTCCTCGATTATATGCTCCAGTTT
TGTCATTAAACTCTCGCTGCTTCTTTTGCATTACTGTCAAAAAGACAGTCTCAACCCTACCCTTTACAAG
ATAACAACGAGGTTGATCATTGCAGTGTAATTGTATAGTGCATTTTAAATTCGTACGGTATTTCGATAAA
TAAATAGAGGCTGGACGTTTGCGATTGCGTCGTCAACTGAA

***wak1+* 3´UTR**

TTACATGGTTTTAGGCGAATGTGTTAACCGCGATTACTACTCGTTCTGCATTCAGTTTAACACGAAATGC
CAAATCTTCGTTGCTTCCTTTAGAAGTGGATGTTGAGTGCATTAGTAATGTTCGTTCTTTAATGTATACT
AAACTATTCAAGGTGAAGGATAATAACAATTTACAGCTTTAATTACAATTAGTCTTTCTGACTTTTTTAA
TGAAATTAAATAGAACATAGTAATGAACTTATATGGAGCAAA

***wis1+* 3´UTR**

AGGTTCGCCTGCTTTCTAATTGCCTGCTCTGTTTTAAAGTACCCATGCGCATTGGTGTTTGTCTTTAATT
TCGAATGCATGACTATTACGTGATCCATAATTATGTTTCAGCAGAACCGACGCTATTTTGCATTTGTGCT
TTTTCATAAATTTAATAATTTGGGTATGATTCCGTATAACGGTAGTTGATGTTTGCATTTTTGCTTTAAA
TTAAAACGGGTATTTAATGTGTTATT

***atf1+* 3´UTR**

ACTGTTTTTGATCTGAAAAGGTCTCAGTCTGTGATGGTTGTAATGAAGAATAACGTTTTTACTTCCCTTT
GACTTTCCCTCCGTTGAGGGTTGTAACGCCCTTTTCCATGCATTTAGCTATGTTATGGATGTGAAATTAT
ATATGTTTATTTTACATTAAAAAATCTTTAGGCTTCTCTTTTTATATTTCTTCCCGTTTTCCATTACTGT
TTTAATTTTGCACTGAACGCCGTCCCGCATGCATACTTTTAGTACTTTATGAAGTGATAAAATTTGTCTG
TCGTGTCTAGTTCACTATAATATCGTTTGGACAACAAAAACTACACGCTTTCTTAATGTTTACCATTCAT
CACATGTGGCAGAGTTATAGAATACTACTTATAACTCATTCTTATGAGATTGATTTGATTTAATAATTAA
AACTATATTATTTAGTAAGAATCAGCAGTGTTTTTAATAACAACTGATTACTGTTTTCCTTTAATGTAAG
AAATCAACAAG

***pyp1+* 3´UTR**

AATTTTTGACTGGATTTTTCTTGGCAATATATATTCGTGTTTTAATCGATTCCTTTATTTCTTGTACTTG
TAAAGTGTCTTTTTTTTTACATTTGCATTTGAATTTACTGTCAATGTTTGTGAAATTCAGTTGCTTTAAT
CACGTTGTCTTTTATTTCAAAAAGTATATTTGAGAACTAGGCTTTTTAATGATATC

***Pyp2+* 3´UTR**

CGAAACGACTGTTCTTTAATTTTCTGTGTTTGTACACACTATGTTCTATTTATGTGAGATTGTGTAATTC
CTCATTTTTTACATTATCTGACGCGAAGGTTATGTTAAAAATACTTAACCACACTCTCCGGTAATCATGT
GTAATTCCTTCCTTATTGTTGTTAAAAATTGATTTTATCTCATGCGTGTAATGAATGTTTATATCTAGTT
ATTAATGAATCTTGTTTATGTTGGAATGGAATAA

Fig. S4

UCAU motifs present at the 3´UTRs sequences corresponding to *wak1+, wis1+, atf1+, pyp1+* and *pyp2+* mRNAs are marked in yellow.

Table S1. *S. pombe* strains used in this study.

Strain	Genotype	Source/Reference
MI200	h$^+$ *pmk1-HA6H::ura4*$^+$ *ade6-M216 leu1-32 ura4D-18*	Madrid *et al.,* 2006
E086	h$^+$ *rnc1::kanR pmk1-HA6H::ura4*$^+$ *ade6-M216 leu1-32 ura4D-18*	This work
MI100	h$^+$ *pmk1::kanR sty1-HA6H::ura4*$^+$ *ade6-M216 leu1-32 ura4D-18*	Madrid *et al.,* 2007
E118	h$^+$ *pmk1::natR rnc1::kanR sty1-HA6H::ura4*$^+$ *ade6-M216 leu1-32 ura4D-18*	This work
MI212	h$^+$ *pmp1::kanR pmk1-HA6H::ura4*$^+$ *ade6-M216 leu1-32 ura4D-18*	Madrid *et al.,* 2007
2119	h$^-$ *his7-336 wis1DD-12myc::ura4*$^+$ *ade6-M216 leu1-32 ura4D-18*	M.A. Rodriguez-Gabriel
E137	h$^+$ *wis1DD-12myc::ura4*$^+$ *rnc1::kanR ade6-M216 leu1-32 ura4D-18*	This work
MM516	h$^+$ *sty1::ura4*$^+$ *pmk1-HA6H::ura4*$^+$ *ade6-M216 leu1-32 ura4D-18*	Madrid *et al.,* 2007
FPR086	h$^-$ *sty1::ura4*$^+$ *rnc1::kanR pmk1-HA6H::ura4*$^+$ *ade6-M216 leu1-32 ura4D-18*	This work
JM1521	h$^+$ *sty1-HA6H::ura4*$^+$ *ade6-M216 leu1-32 ura4D-18*	J.B.A. Millar
E088	h$^-$ *rnc1::kanR sty1-HA6H::ura4*$^+$ *ade6-M216 leu1-32 ura4D-18*	This work
PPG148	h$^-$ *cdc25-22 ura4D-18*	Madrid *et al.,* 2006
FPR176	h$^+$ *cdc25-22 rnc1::kanR ade6-M216 leu1-32 ura4D-18*	This work
FPR483	h$^+$ *his7-336 wak1-9myc::ura4*$^+$ *ade6-M216 leu1-32 ura4D-18*	This work
FPR484	h$^?$ *his7-336 rnc1::kanR wak1-9myc::ura4*$^+$ *ade6-M216 leu1-32 ura4D-18*	This work
E312	h$^+$ *mcs4-GFP::kanR ade6-M216 leu1-32 ura4D-18*	This work
FPR074	h$^+$ *mcs4-GFP::kanR rnc1::natR ade6-M216 leu1-32 ura4D-18*	This work
KS2079	h$^-$ *wis1-12myc::ura4*$^+$ *ade6-M216 leu1-32 ura4D-18*	M.A. Rodriguez-Gabriel
E010	h$^+$ *wis1-12myc::ura4*$^+$ *rnc1::kanR ade6-M216 leu1-32 ura4D-18*	This work
MM1	h$^+$ *ade6-M216 leu1-32 ura4D-18*	Madrid *et al.,* 2006
FPR046	h$^-$ *rnc1::kanR ade6-M216 leu1-32 ura4D-18*	This work
MI701	h$^+$ *pyp1-13myc::kanR ade6-M216 leu1-32 ura4D-18*	Madrid *et al.,* 2007
E090	h$^+$ *pyp1-13myc::kanR rnc1::hygR ade6-M216 leu1-32 ura4D-18*	This work
MI702	h$^+$ *pyp2-13myc::ura4*$^+$ *ade6-M216 leu1-32 ura4D-18*	Madrid *et al.,* 2007
E092	h$^-$ *pyp2-13myc::ura4*$^+$ *rnc1::kanR ade6-M216 leu1-32 ura4D-18*	This work
MI703	h$^+$ *ptc1-13myc::kanR ade6-M216 leu1-32 ura4D-18*	Madrid *et al.,* 2007
FPR078	h$^+$ *ptc1-13myc::kanR rnc1::natR ade6-M216 leu1-32 ura4D-18*	This work
MI1001	h$^+$ *his7-336 pyp1::kanR sty1-HA6H::ura4*$^+$ *ade6-M216 leu1-32 ura4D-18*	Madrid *et al.,* 2007
FPR296	h$^?$ *rnc1::kanR pyp1::kanR sty1-HA6H::ura4*$^+$ *ade6-M216 leu1-32 ura4D-18*	This work
MI704	h$^+$ *pyp2-13myc::ura4*$^+$ *pyp1::kanR ade6-M216 leu1-32 ura4D-18*	Madrid *et al.,* 2007
FPR297	h$^?$ *rnc1::kanR pyp1::kanR pyp2-13myc::ura4*$^+$ *ade6-M216 leu1-32 ura4D-18*	This work
FPR101	h$^+$ *rnc1-3HA::kanR ade6-M216 leu1-32 ura4D-18*	This work
FPR177	h$^-$ *sty1::ura4*$^+$ *sty1-GFP::leu1*$^+$ *ade6-M216 leu1-32 ura4D-18*	This work
FPR183	h$^?$ *sty1::ura4*$^+$ *rnc1-3HA::kanR sty1-GFP::leu1*$^+$ *ade6-*	This work

	M216 leu1-32 ura4D-18	
FPR322	*h$^+$ rnc1(T45AT50AT171AT177AS278AS286A)-3HA::kanR ade6-M216 leu1-32 ura4D-18*	This work
FPR235	h$^+$ *cdc25-22 rnc1-3HA::kanR ade6-M216 leu1-32 ura4D-18*	This work
FPR244	h$^?$ *cdc25-22 rnc1-3HA::kanR pmk1::natR ade6-M216 leu1-32 ura4D-18*	This work
FPR102	h$^?$ *rnc1-3HA::kanR pmk1::natR ade6-M216 leu1-32 ura4D-18*	This work
FPR110	h$^?$ *rnc1-3HA::kanR sty1::ura4$^+$ ade6-M216 leu1-32 ura4D-18*	This work
FPR112	h$^?$ *rnc1-3HA::kanR pmk1::kanR sty1::ura4$^+$ ade6-M216 leu1-32 ura4D-18*	This work
FPR321	h$^+$ *rnc1(K111DA112DR196DN197DR338DG339D)-3HA::kanR ade6-M216 leu1-32 ura4D-18*	This work
FPR197	*h$^+$ cdc10-129 rnc1-3HA::kanR ade6-M216 leu1-32 ura4D-18*	This work
FPR396	*h$^?$ nda3-km311 rnc1-3HA::kanR ade6-M216 leu1-32 ura4D-18*	This work
FPR124	h$^?$ *rnc1-3HA::kanR sty1-HA6H::ura4$^+$ ade6-M216 leu1-32 ura4D-18*	This work
FPR422	h$^?$ *rnc1(K111DA112DR196DN197DR338DG339D)-3HA::kanR sty1-HA6H::ura4$^+$ ade6-M216 leu1-32 ura4D-18*	This work
FPR424	h$^?$ *rnc1(T45AT50AT171AT177AS278AS286A)-3HA::kanR sty1-HA6H::ura4$^+$ ade6-M216 leu1-32 ura4D-18*	This work
FPR122	h$^?$ *rnc1-3HA::kanR pmk1-HA6H::ura4$^+$ ade6-M216 leu1-32 ura4D-18*	This work
FPR423	h$^?$ *rnc1(K111DA112DR196DN197DR338DG339D)-3HA::kanR pmk1-HA6H::ura4$^+$ ade6-M216 leu1-32 ura4D-18*	This work
FPR425	h$^?$ *rnc1(T45AT50AT171AT177AS278AS286A)-3HA::kanR pmk1-HA6H::ura4$^+$ ade6-M216 leu1-32 ura4D-18*	This work
FPR486	h$^?$ *rnc13HA::kanR wak1-9myc::ura4$^+$ ade6-M216 leu1-32 ura4D-18*	This work
FPR489	h$^?$ *rnc1(K111DA112DR196DN197DR338DG339D)-3HA::kanR wak1-9myc::ura4$^+$ ade6-M216 leu1-32 ura4D-18*	This work
FPR492	h$^?$ *rnc1(T45AT50AT171AT177AS278AS286A)-3HA::kanR wak1-9myc::ura4$^+$ ade6-M216 leu1-32 ura4D-18*	This work
FPR416	h$^?$ *rnc13HA::kanR wis1-12myc::ura4$^+$ ade6-M216 leu1-32 ura4D-18*	This work
FPR417	h$^?$ *rnc1(K111DA112DR196DN197DR338DG339D)-3HA::kanR wis1-12myc::ura4$^+$ ade6-M216 leu1-32 ura4D-18*	This work
FPR418	h$^?$ *rnc1(T45AT50AT171AT177AS278AS286A)-3HA::kanR wis1-12myc::ura4$^+$ ade6-M216 leu1-32 ura4D-18*	This work
FPR426	h$^?$ *rnc1-3HA::kanR pyp1-13myc::kanR ade6-M216 leu1-32 ura4D-18*	This work
FPR427	h$^?$ *rnc1(K111DA112DR196DN197DR338DG339D)-3HA::kanR pyp1-13myc::kanR ade6-M216 leu1-32 ura4D-18*	This work
FPR428	h$^?$ *rnc1(T45AT50AT171AT177AS278AS286A)-3HA::kanR pyp1-13myc::kanR ade6-M216 leu1-32 ura4D-18*	This work

FPR429	h? *rnc1-3HA::kanR pyp2-13myc::kanR ade6-M216 leu1-32 ura4D-18*	This work
FPR430	h? *rnc1(K111DA112DR196DN197DR338DG339D)-3HA::kanR pyp2-13myc::kanR ade6-M216 leu1-32 ura4D-18*	This work
FPR431	h? *rnc1(T45AT50AT171AT177AS278AS286A)-3HA::kanR pyp2-13myc::kanR ade6-M216 leu1-32 ura4D-18*	This work

Table S2. Oligonucleotides and DNA fragments used in this study.

OLIGONUCLEOTIDE	SEQUENCE 5'-3'	Use
Rnc1D-FWD	AATTTAGAAAAGGTTCTACTCTCCTCCTAGAAACGCATATGTGTCCTATTCAATTAACCAATACTATTCCAGTGACATCTCGGATCCCCGGGTTAATTAA	*rnc1*$^+$ deletion
Rnc1D-REV	ACACAAGTCCAAAAAAATCTAGCAAACAAGAGAGAATACCTTGGATGCAAAACCAAAGTACGAAGGCAAGTACTAAGAGTGAATTCGAGCTCGTTTAAAC	*rnc1*$^+$ deletion
Rnc1D-COMP FWD	ACTTCCTATCAGTAAATTGTCGAC	Confirmation of *rnc1*$^+$ deletion
Rnc1-CT-FUSION-FWD	ACACACGAGGAAAATGAGAAAGCCCTTTTCTTACTCTACCAGCAATTAGAAATGGAAAAAGATCGTCGTTCTCATCGGATCCCCGGGTTAATTAA	*rnc1*$^+$ C-terminal tagging
Rnc1-CT-FUSION-REV	TGTGACACCACTAGTTAAACTAAACCAAATTTTTACAAAACATTGATGAACGGGAAAGGGGAAAAGCAAAAGGATAAACTGAATTCGAGCTCGTTTAAAC	*rnc1*$^+$ C-terminal tagging
Rnc1-CT-COMP-F	GTTGGTTGTATAATAGGTCGTGGAG	Confirmation of *rnc1*$^+$ tagging
KAN-COMP-R	GATGTGAGAACTGTATCCTAGCAAG	Common oligonucleotide for confirmation of gene tagging
Rnc1-Casette FWD	TTCACTTCCAAAGATATAACGACTGAGGCG	C-terminal tagged *rnc1*$^+$cassette amplification, cloning and sequencing
Rnc1-Casette REV	CCAATATTCATGCAACAACGTATAGAGCTG	C-terminal tagged *rnc1*$^+$cassette amplification and cloning
Rnc1-Seq1 FWD	CAAGTCTCCCCTCCAGCAGCTCCC	*rnc1*$^+$ sequencing
Rnc1-Seq2 FWD	TTCTATGAACTGCGGTGTTACATAG	*rnc1*$^+$ sequencing
Rnc1-T50A-FWD	CATTGCTAAAGTTTCCATACCTACTCCAAAGCCCTCTGCACCTCTATCGACTCTTACTAACGGTTCTACTATTCAACAGT	Rnc1 threonine-50 replaced by alanine (site-directed mutagenesis)
Rnc1-T50A-REV	ACTGTTGAATAGTAGAACCGTTAGTAAGAGTCGATAGAGGTGCAGAGGGCTTTGGAGTAGGTATGGAAACTTTAGCAATG	Rnc1 threonine-50 replaced by alanine (site-directed mutagenesis)
GSTRnc1-FWD-BamHI	TTAATGGATCCATGGCTTACAATCACTTCAGCATTC	Cloning of *rnc1*$^+$ ORF into pGEX-KG
GSTRnc1-REV-XbaI	TTAATTCTAGATCAATGAGAACGACGATCTTTTTCC	Cloning of *rnc1*$^+$ ORF into pGEX-KG
GSTSty1-FWD-SmaI	TTAATCCCGGGAATGGCAGAATTTATTCGTACACAAAT	Cloning of *sty1*$^+$ ORF into pGEX-KG
GSTSty1-REV-XbaI	TTAATTCTAGAATGGATTGCAGTTCATTATCCATGTTG	Cloning of *sty1*$^+$ ORF into pGEX-KG
GST-REV-BamHI	TTAATTCTAGATCAGTCACGATGAATAAGCTTGAG	Cloning of GST and GST tagged *rnc1*$^+$ into pREP3X
GST-FWD-XhoI	TTAATCTCGAGATGTCCCCTATACTAGGTTATTGGA	Cloning of GST and GST tagged *rnc1*$^+$ into pREP3X
GST-Rnc1-REV-SmaI	TTAATCCCGGGTCAATGAGAACGACGATCTTTTTCC	Cloning of GST and GST tagged *rnc1*$^+$ into pREP3X
Leu1-FWD	CTTCCCTTCTCCTTCGTTATGG	q-PCR
Leu2-REV	CCTCCCAAATCGCGAGTATAAA	q-PCR
Mcs4-FWD	TTTCCTCGGAGGTTGCTAAAG	q-PCR
Mcs4-REV	CATCGTGGGAAGTTGGATGT	q-PCR
Wis4-FWD	AAACCCAGAAGCACTGAAGG	q-PCR
Wis4-REV	CTATCGGATGAACGGGACATAAA	q-PCR
Win1-FWD	TGATACGACAAAGGAGAACAGG	q-PCR
Win1-REV	CCGAAAGAACCGCTACCTATAA	q-PCR

Wis1-FWD	ATCTGGCTCTTCGTTTCGTATT	q-PCR
Wis1-REV	GTCGGTTGATGCAATGCTTTAT	q-PCR
Sty1-FWD	ATGACGGGCTATGTTTCTACTC	q-PCR
Sty1-REV	ATACAACCCGCACTCCAAATA	q-PCR
Atf1-FWD	TCACCTGGTACTGCCAATTTAT	q-PCR
Atf1-REV	CCATTTACAACAGGCGGTTTAC	q-PCR
Pyp1-FWD	GAAGGCTCCGATTACTTCTCTC	q-PCR
Pyp1-REV	TGTTGTCCTTGTTCTCAGGTAG	q-PCR
Pyp2-FWD	CTACGATCGGTGCCTTCTTATC	q-PCR
Pyp2-REV	TGACGACGTTGCTGGATTTA	q-PCR
Ptc1-FWD	CGCTGCAGTTGCTTTCTTTAG	q-PCR
Ptc1-REV	GCCTTACCATCACGGCATAATA	q-PCR
Ptc3-FWD	CGTACTCGCTTGTGATGGTATT	q-PCR
Ptc3-REV	AAGAGAGGTTCCAGCAACTATG	q-PCR
Pmp1-FWD	GGATAGGTCCCAACATGTCTTT	q-PCR
Pmp1-REV	TTCAAGGATGACGATTGATAGGG	q-PCR

gBLOCKS GENE FRAGMENT	**SEQUENCE 5'-3'**	**Use**
Rnc1 (T45A, T50A, T171A, T177A, S278A, S286A) SacI/PacI	TATTA*GAGCTC*TTCACTTCCAAAGATATAACGACTGAGGCGTAAAG CTACGCTACCACTTCCTATCAGTAAATTGTGCGACTTTACTATACGT TCTTCAAACTTCGTTATTTCCCCACCAAAAGACTTACTTGCAGAAAA TTTTCTCTTTGTCACTGCTACACCCCGTTTACCACTACTCCGTTCTC CTTGGTCGTTTACTTCATTTTTGTCGAAGTAATCACAGCTATTGATT GCAATTTCAATTTATAAGAAACTGCAATAAGAGCTTAGAAGGAGCCT AATCCGTTTTCCTTTTTTTTTTTTAATCTCCGCTAAATCCCTGCAGGTT TGAACTAATCAGTTTTCAGGAAGTAATTTAGAAAAGGTTCTACTCTC CTCCTAGAAACGCATATGTGTCCTATTCAATTAACCAATACTATTCC AGTGACATCTATGGCTTACAATCACTTCAGCATTCCTAAAAACATCG AGGAAAAAGAGAACTCTTTTTTTGACGTAACGTTTCAAGACGAACC CGACGAAACCACTTCTACTGCTACTGGCATTGCTAAAGTTTCCATA CCT*GCT*CCAAAGCCCTCT*GCA*CCTCTATCGACTCTTACTAACGGTT CTACTATTCAACAGTCCATGACCAACCAACCCGAACCAACGTCTCA AGTGCCTCCCATCTCTGCCAAGCCACCGATGGATGATGCCACCTAT GCTACTCAACAACTTACCTTGAGAGCCTTACTTTCTACTCGTGAAG CTGGTATCATTATTGGTAAAGCTGGAAAAAACGTTGCCGAACTCAG AAGCACTACAAATGTCAAGGCCGGCGTTACCAAGGCTGTTCCTAAT GTTCATGATCGTGTTTTAACTATTAGTGGACCACTAGAGAATGTTGT TCGCGCTTATAGATTCATCATCGATATTTTTGCCAAGAACAGTACTA ACCCTGATGGT*GCA*CCTTCCGACGCCAAC*GCA*CCTCGCAAACTTC GTCTTTTGATCGCCCATTCTCTGATGGGTAGTATTATTGGCCGCAA TGGTTTGCGTATCAAGCTTATTCAGGACAAATGTAGTTGCCGTATG ATTGCTTCCAAAGACATGCTTCCACAGTCTACTGAGCGTACAGTTG AAATCCATGGTACAGTCGATAATCTTCATGCTGCCATTTGGGAAATT GGCAAATGCTTAATTGATGACTGGGAGCGTGGCGCCGGTACCGTT TTCTATAATCCCGTTTCTCGTTTGACTCAACCTCTTCCTTCTCTTGC GTCGACTGCA*GCT*CCTCAACAAGTC*GCC*CCTCCAGCAGCTCCCTC CACGACTTCTGGTGAAGCTATCCCCGAAAACTTTGTTTCTTACGGT GCTCAAGTCTTTCCAGCTACCCAAATGCCTTTCTTGCAGCAACCTA AGGTTACCCAAAATATTAGCATTCCCGCAGATATGGTTGGTTGTATA ATAGGTCGTGGAGGATCTAAGATTTCGGAAATCCGTCGTACCAGC GGTAGCAAGATTTCCATTGCCAAAGAACCTCATGATGAGACAGGCG AACGTATGTTCACCATTACAGGTACACACGAGGAAAATGAGAAAGC CCTTTTCTTACTCTACCAGCAATTAGAAATGGAAAAAGATCGTCGTT CTCATCGGATCCCCGGG*TTAATTAA*CATCT	Cloning into plasmid pTA-Rnc1:HA to obtain MAPK non-phosphorylatable Rnc1 mutant
Rnc1 (K110D, A111D,	TATTA*GAGCTC*TTCACTTCCAAAGATATAACGACTGAGGCGTAAAG CTACGCTACCACTTCCTATCAGTAAATTGTGCGACTTTACTATACGT	Cloning into plasmid pTA-Rnc1:HA to obtain non-

R196D, N197D, R338D, G339D) SacI/PacI	TCTTCAAACTTCGTTATTTCCCCACCAAAAGACTTACTTGCAGAAAA TTTTCTCTTTGTCACTGCTACACCCCGTTTACCACTACTCCGTTCTC CTTGGTCGTTTACTTCATTTTTGTCGAAGTAATCACAGCTATTGATT GCAATTTCAATTTATAAGAAACTGCAATAAGAGCTTAGAAGGAGCCT AATCCGTTTTCCTTTTTTTTTTTTAATCTCCGCTAAATCCCTGCAGGTT TGAACTAATCAGTTTTCAGGAAGTAATTTAGAAAAGGTTCTACTCTC CTCCTAGAAACGCATATGTGTCCTATTCAATTAACCAATACTATTCC AGTGACATCTATGGCTTACAATCACTTCAGCATTCCTAAAAACATCG AGGAAAAAGAGAACTCTTTTTTTGACGTAACGTTTCAAGACGAACC CGACGAAACCACTTCTACTGCTACTGGCATTGCTAAAGTTTCCATA CCTACTCCAAAGCCCTCTACACCTCTATCGACTCTTACTAACGGTT CTACTATTCAACAGTCCATGACCAACCAACCCGAACCAACGTCTCA AGTGCCTCCCATCTCTGCCAAGCCACCGATG*GATGAT*GCCACCTAT GCTACTCAACAACTTACCTTGAGAGCCTTACTTTCTACTCGTGAAG CTGGTATCATTATTGGT*GATGAT*GGAAAAAACGTTGCCGAACTCAG AAGCACTACAAATGTCAAGGCCGGCGTTACCAAGGCTGTTCCTAAT GTTCATGATCGTGTTTTAACTATTAGTGGACCACTAGAGAATGTTGT TCGCGCTTATAGATTCATCATCGATATTTTTGCCAAGAACAGTACTA ACCCTGATGGTACACCTTCCGACGCCAACACACCTCGCAAACTTCG TCTTTTGATCGCCCATTCTCTGATGGGTAGTATTATTGGCGACGAT GGTTTGCGTATCAAGCTTATTCAGGACAAATGTAGTTGCCGTATGA TTGCTTCCAAAGACATGCTTCCACAGTCTACTGAGCGTACAGTTGA AATCCATGGTACAGTCGATAATCTTCATGCTGCCATTTGGGAAATT GGCAAATGCTTAATTGATGACTGGGAGCGTGGCGCCGGTACCGTT TTCTATAATCCCGTTTCTCGTTTGACTCAACCTCTTCCTTCTCTTGC GTCGACTGCAACTCCTCAACAAGTCTCCCCTCCAGCAGCTCCCTCC ACGACTTCTGGTGAAGCTATCCCCGAAAACTTTGTTTCTTACGGTG CTCAAGTCTTTCCAGCTACCCAAATGCCTTTCTTGCAGCAACCTAA GGTTACCCAAAATATTAGCATTCCCGCAGATATGGTTGGTTGTATAA TAGGT*GATGAT*GGATCTAAGATTTCGGAAATCCGTCGTACCAGCGG TAGCAAGATTTCCATTGCCAAAGAACCTCATGATGAGACAGGCGAA CGTATGTTCACCATTACAGGTACACACGAGGAAAATGAGAAAGCCC TTTTCTTACTCTACCAGCAATTAGAAATGGAAAAAGATCGTCGTTCT CATCGGATCCCCGGG*TTAATTAA*CATCT	mRNA binding (KH domains) Rnc1 mutant